

On the sub-synoptic scale meteorology of two extreme fire weather days during the
Eastern Australian fires of January 2003

Graham A. Mills

Bureau of Meteorology Research Centre

July 2005

Abstract

During January and February 2003 vast areas of Australia's Alpine areas were burnt during a series of massive bushfires. In this paper the synoptic evolution and mesoscale circulation systems that led to extreme fire weather on January 18, the day the fires devastated the Australian Capital Territory, and January 30, the day the Alpine fires "broke out" in the Victorian high country are discussed. In each case the extreme fire weather experienced was associated with a "cool change" passage, but the strongest winds are shown to be associated with mesoscale wind maxima generated near the top of the mixed layer, which in these cases was 2000-4000 m deep. The surface structures of the cool changes were strongly affected by diabatic heating, and it is shown how these diabatic processes cause the structure of these changes to vary strongly over relatively short distances. On January 18 an additional feature was a series of progressive reductions in humidity at and in the areas surrounding Canberra. Reasons for this behaviour are discussed, and the role of a mid-tropospheric dry slot identified in water vapour imagery, and a possible contribution from cross-frontal circulations, are described.

Introduction

During January and February 2003 vast areas of Australia's Alpine areas were burnt during a series of massive bushfires (see Fig. 1 in Bureau of Meteorology 2003). While not minimising any part of the period, two days stand out meteorologically. The first was 18 January 2003, when fires caused the deaths of four people, many other injuries, the loss of over 500 houses and other infrastructure losses, and more than 70% of the parks, forests and pastures in the Australian Capital Territory (ACT) was burnt (McLeod 2003) (see Fig.1 for place names referred in the text, and for the topography of the region). The second day was 30 January 2003, when strong, gusty winds over the Victorian Alpine country, associated with high temperatures and low humidity, contributed to the Eastern Victorian fires making major "runs" to the southeast (see Bureau of Meteorology, 2003). On each day wind changes were expected in the area of the fires, with a change from northwesterly to southeasterly winds expected in Canberra in the evening of 18 January, while a "cool change" was progressing through Victoria on 30 January. In each case, though, very strong and gusty winds were experienced in the pre-change airmass, with wind gusts around 40 kn being experienced at Canberra Airport during the afternoon of 18 January, and a sustained period of mean wind speeds between 30 and 40 kn, with gusts between 45 and 55 kn at Mt. Hotham from the early morning to the late afternoon of January 30. While many cool changes contribute to extreme fire weather in southeastern Australia, significant features of these two cool changes did not fit the many published conceptual models of frontal structure (see, for example those referenced in Mills 2002), or at least the surface evolution of wind and temperature associated with these conceptual models.

The first aim of this paper is to document the synoptic and mesoscale meteorology of these two events. The second aim is to describe and diagnose in some detail the sub-synoptic circulation systems that led to the extreme fire weather on those two days. While these features are not identifiable from mean-sea-level pressure forecasts, it will be shown that even with relatively simple diagnostic techniques useful guidance for these events can be provided by operational mesoscale NWP models. These diagnostic techniques can then be used to identify the mesoscale

features leading to this surface gustiness, potentially providing improved forecast services to fire agencies.

As stated above, on each of these two days wind changes, or cool changes, were forecast through the respective fire zones of southeastern Australia, where the topography is significant and is commonly considered to have a blocking effect on the movement of these cool changes. Considerable research effort has been expended in investigating the structure and movement of cool changes through southeastern South Australia and western Victoria, including the phenomena of “coastal surging” of fronts along the coastline west of Melbourne (see the references quoted in Mills 2002). A further considerable effort has investigated the so-called “southerly burster” – a rapidly propagating cold front moving northwards along the New South Wales (NSW) coastline (Colquhoun et al 1985), and it is recognised that the blocking effect of the Great Dividing Range in far eastern Victoria and southern New South Wales is an essential component in the development of the southerly burster. However, there has been little published describing the inland structure and behaviour of these cool changes, or their modification by the topography of southeastern Australia, since the works by Clarke (1983). That study, and Clarke’s earlier observational studies, describe the passage of late evening “wind surges” through Canberra and Wagga as more related to inland sea-breeze propagation rather than a cold frontal passage. Morgan (2002) also points to the difficulty of identifying the passage of cool changes at elevated sites such as Mt. Hotham. This paper provides a description of the behaviour of two “frontal” passages over and inland of the elevated terrain of southeastern Australia, and thus adds to the very small number of such descriptions.

In the two main sections of this paper, the 18 January and 30 January events will be described in some detail. In each case, the evolution of the wind, temperature, and humidity at several stations in the area of the respective fires will be described, highlighting the common and different features occurring over relatively small areas, and particularly those features that do not necessarily fit established paradigms of cool-change morphology over southeastern Australia, and yet had significant impact of the fire weather of each of those days. A synoptic description of each event over a 30-hour period will document the larger-scale environments of the two cases, and provide background to the mesoscale diagnosis that follows. The mesoscale diagnosis

will describe the structures and evolution of the small-scale thermal gradient and wind speed maxima that occurred near the top of the well-mixed boundary layer, and which are hypothesised to be the source of the maxima in surface gustiness observed on these two days. As part of this diagnosis, some products that provide potentially useful forecast guidance are presented.

Techniques and data sources

Data sets

The principal diagnostic data used in this study are the archive of operational NWP products produced by the Bureau of Meteorology's operational LAPS system (Puri et al 1998). The system has a hierarchy of internally nested forecast areas, with the largest scale region having a 3-cycle intermittent data insertion cycle before the forward forecast, and a horizontal grid spacing of 0.375° . Internal meshes with horizontal grid spacing of 0.125° covering all of Australia, and of 0.05° centred over Melbourne and Sydney are nested inside the coarser mesh, and use the coarser mesh analyses to provide the initial state. Each forecast model uses the same 29-level vertical discretisation in sigma coordinates, and the same suite of physical parameterisations. In this paper the respective strengths of the different systems will be used to emphasise different aspects of the two cases. The 0.375° analyses, available at 6-hourly intervals, will be used to provide the synoptic descriptions, with their strength being the close matching of observations coupled with the dynamic balance achieved during the data assimilation cycles. The 0.125° model and the 0.05° model outputs contain internally generated dynamic and temporal consistency at scales finer than those allowed by the correlation functions used in the analyses. The 0.125° model covers a wide area, and has archived tropospheric fields every 3 hours, while the 0.05° model runs have these fields archived every hour, allowing greater time resolution at the expense of lesser geographic coverage. While the finer-scale model outputs contain greater spatial and temporal detail than do the analyses, it must be remembered that they are forecasts, and so comparison of these forecasts with verifying observations is vital in order to support the inferences drawn from diagnosis of these model outputs. Hourly and half-hourly data from the Bureau's AWS network, and some radiosonde data, are used to perform this function.

There is one exception to the use of operational NWP products. The operational analysis used to initialise the forecast for the 18 January 2003 event showed an unusual surface mixing ratio pattern associated with a “bug” in the objective analysis code. In order to ensure that this did not affect the conclusions drawn in the diagnostic part of the paper, a hindsight assimilation and 0.05° model run was prepared using analysis codes that had corrected the moisture analysis bug, and which were implemented operationally on 13 February 2003 (P. Steinle 2004, personal communication). There was very little difference between the wind and temperature fields in this model run and those in the operational forecast, but the moisture fields did show some differences, and it is this hindcast rather than the operational 0.05° forecast that will be used in the later parts of this paper.

Diagnosis of gusts from NWP data

A variety of methods have been proposed over the years to diagnose the gust at anemometer height from larger-scale atmospheric parameters such as those forecast from NWP models. Brasseur (2001) argues from physical grounds that gusts at the surface are the result of turbulence mixing momentum from higher to lower levels, and so the highest gust likely at a near-surface level is that from the level at which the wind speed is highest, and where the turbulent kinetic energy is sufficient to overcome the buoyancy forces in the atmospheric column below that level, providing a simple physical model in cases when a clearly identifiable well-mixed boundary layer can be identified. Verkaik (2000) discusses two alternative methods based on the probability distribution of turbulent statistics (the method proposed by Weiringa (1986) depends on empirical gust and horizontal wind speed standard deviation data, while that proposed by Beljaars (1987) depends on empirical horizontal wind speed power spectra data). Adopting the formulation of Beljaars (1987) and integrating over the frequency domain produces a formula for the 3-second wind gust at 10 m. This formula is based on the model’s 10 m wind speed, the friction velocity, the stability, and the atmospheric stability (ie the ratio of the boundary layer depth to the Obukhov length). The Beljaars formulation has been applied in this paper to the NWP model output, and the forecast gust products shown in the later sections have been derived

using this method, although qualitatively very similar and quantitatively comparable forecasts are obtained using the physical model.

Definitions of a front

There are many references to “the front” or to the “cool change” in the descriptions to follow. Hewson’s (1998) definition of a front as “the warm-air boundary of a zone of enhanced thermal gradient”, subject to the thermal gradient being of sufficient strength, is that used in this paper. This definition places the front at the point where significant cooling begins and is also where NWP model output places the abrupt wind change, as shown in Mills (2002, 2005), and has been found to be the most appropriate definition when applied to dry summertime fronts over southeastern Australia. Particularly in the later description of NWP model forecasts, the term “front” will be used in this context, while the term “trough” will be used when pressure fields are being described, although there is, of course, a close dynamic relationship between the two.

January 18 – synoptic description

Figure 2 shows the MSLP analyses at 6-hourly intervals from 0600 UTC 17 January to 1200 UTC 18 January 2003. At the initial time (Fig. 2a) a broad trough is located over southeastern Australia, with one weakly defined axis from northern South Australia (SA) to the far southeast of NSW, and another north-south axis along the Victorian-SA border. A large high is in the Tasman Sea, and a ridge of high pressure extends from the Bight to Tasmania. In the southwest of the plotted area there is a mid-latitude trough in the westerlies.

During the subsequent 18 hours, the mid-latitude trough moved eastwards, and linked with the trough over the continent to form a low over southeastern NSW and a sharp trough over Tasmania (Fig. 2c). With this eastward movement of the mid-latitude pressure systems, the Bight high strengthened along ~ 40S, leading to strengthening pressure gradients over Tasmania and Victoria and a narrow ridge extending through Bass Strait by 0000 UTC 18 January (Fig. 2d). After 0000 UTC (Fig. 2e,f) the narrow ridge through Bass Strait extended northwards along the NSW

coast in a “southerly burster” (Colquhoun et al, 1985) like pattern, while the low over southeastern NSW moved northeast and was located just off the NSW coast north of Sydney by 1200 UTC 18 January. A heat/lee low had formed over Tasmania by 0600 UTC 18 January (Fig. 2e) (see Mills and Pendlebury 2003 for a discussion of such lows).

During this period the upper tropospheric analyses show a relatively weak pattern over the Australian continent (Fig. 3) with anticyclonically-curved height contours over southeastern Australia, and a weak mid-latitude trough in the south of the plotted area.

It is instructive to relate the surface temperature and near-surface wind flows and the evolving pressure patterns. Figure 4 shows analyses of screen-level potential temperature (used rather than temperature to reduce the topographic influence, and thus to display the larger-scale evolution more clearly), and near-surface wind speed and direction. At 0000 UTC 18 January (Fig. 4a) there is a zone of strong temperature gradient at screen level along the eastern and southeastern Australian coasts. North of Cape Howe, there is a quite marked cyclonic curvature in the wind field across this coastal gradient, and this has some similarities to the “coastal warm front” seen off the Victorian coast in the case described by Mills (2005), as a strong, hot offshore flow develops a stable internal boundary layer after moving over a cooler sea surface. Immediately west of Cape Howe a strong temperature gradient lies parallel to the Great Dividing Range, and a cool change (the zone of temperature gradient) is oriented northwest-southeast across southern NSW, from the SA border to the ranges. Winds across this front are cyclonically curved, and oriented directly from cool to warm air, and so adiabatic cool advection is occurring in this area. There is also a zone of enhanced temperature gradient extending along the western Victorian and the SA coastlines associated with the land-sea boundary, but based on its subsequent evolution, this has less dynamic significance than the zones of stronger thermal gradient described earlier in this paragraph.

In the subsequent 12 hours (Figs. 4b,c) the cool change over inland NSW moved northeastwards with winds backing and freshening, the cool air south of the eastern Victorian ranges extended slowly northwards. Given that the temperature

contours represent the *screen level* potential temperature, the cool air boundary can only advance northwards as the depth of the post-frontal cool air increases to reach the height of the topographic barrier here (Fig. 4d). The southerly burster moved northward along the NSW coastline after 0000 UTC (Fig. 4e,f), and with the development of this on-shore directed pressure gradient the winds backed, advected cooler maritime air inland, and consequently the coastal temperature gradient moved inland. The net result is a narrowing and northward movement of the zone of hot air that was over southeastern NSW at 0000 UTC as what might be interpreted as three separate cool changes advance from the southwest, south, and east.

January 18 – an observational perspective

The time-series of observations at Canberra Airport shows fascinating evolution during 18 January 2003 (Fig. 5). Winds were light and variable overnight, but with the onset of daytime heating after 1930 UTC the wind direction settled to the north and then slowly backed to the northwest. The gust factor increased from around 2200 UTC, and both mean speed and gusts rose to a dramatic peak at around 0430 UTC. Thereafter the speed and gust decreased until the arrival of an easterly change at 0800 UTC. After this change, the wind speed increased again to nearly 20 kn, with gusts approaching 30 kn. The relation between the temperature, the wind speed and the dewpoint time-series is interesting. The initial increase in wind speed coincides with the commencement of daytime heating and is consistent with the breaking of a nocturnal surface inversion. However at around 0000 UTC the speed and gustiness further increased steadily for some hours and coinciding with this there was a decrease in dewpoint, which might be interpreted as a mixing of low- to mid-tropospheric air as the daytime mixed layer depth increased. The wind speed and gustiness decreased markedly after 0430 UTC, but with little change in wind direction during this period. There were however, two further marked decreases in humidity – one at 0300 UTC, when the dewpoints decreased from 4C to –3C, and a second very marked drying from 0530 to 0700 UTC, when dewpoints decreased to –13C. The abrupt arrival of the easterly wind change at 0800 UTC is marked by an increase of wind speed and gustiness immediately after the change, and a rapid increase in dewpoint and a decrease in temperature, showing the effects of the inland penetration of the cooler air propagating northward along the NSW coastline (Fig. 4).

Some commentaries on the event (eg McLeod 2003, p42) have hypothesised that the gustiness in the mid-afternoon and the abrupt drying in the late afternoon were associated with the convection column above the fire west of Canberra, and so was fire-driven. Meteograms of observations at elevated stations in the region surrounding Canberra, where observations are available at Thredbo (1957m), Cooma (930m), Cabramurra (1482m), and Goulburn (640m) (Fig. 6) may be compared with the Canberra meteograms in Fig. 5. All these stations show a similar pattern, with a maximum in wind speed and gustiness in the mid-afternoon, a sudden dramatic drying after the wind speed has begun to decrease, and an abrupt wind change to the southeast in the evening with decreasing temperatures and increasing humidity. Clearly the gustiness and the abrupt and dramatic decreases in humidity at Canberra were the response to significantly larger scale atmospheric flow features than would be the case had the drying been induced by subsidence associated with the pyrocumulus cloud west of Canberra. There is some suggestion that the drying occurred earlier in the south and east and later in the north and west, indicating that the circulation features that led to the drying were coherent and northward/westward moving. In the next section mesoscale model output will be used in an attempt to diagnose these structures, and address their predictability.

January 18 – mesoscale diagnosis

First the verisimilitude of the NWP model prediction (in this case the 0.05° Sydney region meso-LAPS hindcast) for Canberra Airport is examined, for comparison with the observed meteograms in Fig. 5. Figure 7 shows the forecast meteograms. The model has produced a quite outstanding forecast of most elements. Temperatures commence rising at 2000 UTC, and shortly after that time the wind direction settles to the north-northwest and wind speed and gust both commence a steady increase. Shortly after the temperature begins to climb, the dewpoint falls to around 1C and shows two shallow minima around 0300 UTC and just before the easterly change at 0800 UTC. The forecast gustiness of >35 kn between 0200 and 0700 UTC with a peak of 39 kn at 0500 UTC matches well the observed peak of 42 kn at 0500 UTC, and the timing of the easterly change is as close as possible given the hourly output interval from the model.

There are some aspects of the forecast that are not perfect – the mean wind speed is lower than observed, a feature characteristic of many NWP models where the grid-square average wind and roughness (particularly over mountainous terrain where roughness lengths are enhanced) is at odds with the characteristics of a “well-exposed” anemometer site. In addition, while shallow minima in the dewpoint forecast are seen in the late afternoon, the forecast does not show the amplitude of drying seen in the observations. However, the model-based diagnosis of the mesoscale circulations around Canberra on the afternoon of January 18 will proceed on the assumption that the model is sufficiently accurate in many of its features to provide useful insight, while the humidity forecast will be discussed further later.

The diagnosis of near-surface gustiness using Beljaars’(1987) formulation and shown in Fig. 7 is remarkably accurate given that it is based on forecast fields. These results are consistent with the physically-based hypothesis that the strongest wind speed in the mixed layer may be realised as maximum surface gust, and this is also supported by the Wagga rawinsonde ascent at 0000 UTC 18 January (Fig. 8). This shows a deep, near adiabatic boundary layer extending to approximately 600 hPa, although only between 700 and 600 hPa does the mixing-ratio indicate that the layer is well-mixed. A very significant feature though, is the 50 kn wind maximum just below the sharp reduction in humidity and transition to slightly greater thermal stability near 600 hPa which is interpreted to mark the top of the mixed layer. If this profile were to be realised by the numerical model, then it is entirely plausible that this 50 kn wind would be realised as the surface gust value.

Figure 9 shows the time-sequence of the 700 hPa temperature field and overlaid wind speed field forecasts from the meso-LAPS 0.125° model (used here because the western boundary of the 0.05° grid Sydney domain model is at 147E). An isolated 700 hPa short-wave temperature trough had generated an east-west zone of enhanced temperature gradient along the Victorian-NSW border at 2100 UTC (Fig. 9a), and reflecting this lower-tropospheric temperature gradient an isotach maximum developed in response. Over the next 9 hours (Figs. 9b-d) the short-wave temperature trough contracted eastwards and moved slowly northwards together with the isotach maximum. Below this level the forecast atmosphere is well mixed to the surface and it

is thus the passage of this isotach maximum that produces the forecast gustiness maximum at Canberra in Fig. 7, and thus may be hypothesised to have been the main contributor to the observed gustiness.

Diagnosis of the possible reasons for the extreme drying occurring at elevated stations in southeastern NSW on 18 January 2003 is the final point to be addressed in this section. Concentrating on the Canberra meteograms (Fig. 5), it is hypothesised that the initial steady dewpoint decrease commencing around 2330 UTC is due to mixing of dryer air from above, as it commences as the temperature has increased and with the increased wind speed and gustiness. Figure 10 shows water vapour channel ($6.7\mu\text{m}$) imagery at four times during 18 January. At 2330 UTC a dark band is seen across southwestern NSW. Such dark bands are frequently associated with low mid-tropospheric humidities (Weldon and Holmes 1991) and this is supported by the cross-section (Fig. 11) along the line shown in the upper panel of Fig. 10. This shows a minimum in mixing ratio in the middle of the section, where the imagery would suggest such a minimum should be located. The lower panels of Fig. 10 show this dry band moving eastwards and northwards across NSW during 18 January, reaching the Canberra area around 0400 UTC, and it is proposed that mixing of this dryer air to the surface led to the second decline in humidity at Canberra. Lower-elevation observations also showed a marked drying associated with the passage of this dry band, as is shown, for example, at Wagga (Fig. 12) where dewpoints drop from -6C to -22C between 0130 and 0330 UTC, and its south-to-north movement over southeastern NSW is consistent with the trend seen in the observations of Figs. 5 and 6.

Turning now to the third decline in dewpoint between 0530 and 0730 UTC, the $.05^\circ$ Sydney region meso-LAPS hindcast is used for its high spatial and temporal resolution. Figure 13 shows forecasts of potential temperature and wind for 0500 UTC 18 January, and the thermal gradient and strong convergence line between the southeasterly change moving inland from the coast and the hot westerly winds over the interior of NSW are clearly seen. Much weaker, but still discernable, are the temperature change associated with the shift to southwesterly winds inland of the NSW ranges, and the southerly push over the ranges. The forecast screen-level

dewpoint at the same time (Fig. 14) shows a northwest-southeast oriented dewpoint minimum in the north of the plotted area, and this is hypothesised to be associated with the dry band seen in the water-vapour imagery. A very strong moisture gradient is associated with the easterly wind change, and oriented along the moisture front, on the dry side, is an elongated local minimum extending over some considerable distance. A vertical cross-section section (Fig. 15), approximately normal to the easterly change line, shows the deep mixed layer in the inland portion of the section, together with the local wind speed maximum just above the top of that layer, and also shows the front approaching Canberra from the east, with strong ascent at the head of the front and strong temperature and mixing ratio gradients immediately east of the front. West of the front there is an area of only weak, or neutral vertical motion, and immediately west of the front there is a narrow zone of relatively dryer air, marked by the 4.5 gm/Kg isopleth. The spatial coherence of this local dewpoint minimum, in conjunction with its temporal consistency through the forecast and the vertical structure seen in the cross-section, does suggest that it has an association with the easterly change. Further, its westward movement and the orientation of the temperature/humidity gradient is consistent with the apparent later westward/northward arrival times of the drying event seen in the observations (Figs. 5,6). It thus appears that the final drying period was associated with the frontal circulations of the easterly cool change.

If the above hypotheses are correct, however, then perhaps the forecast dewpoints should have been more accurately forecast (Fig. 7). The width of the dry band parallel to the easterly change in Fig. 15 is of the order of 10-20 km. Given that the grid-spacing of the model is of the order of 5 km, it might be expected that the model would fail to resolve the amplitude of such a feature. The speed of advance of the easterly change is around 8 km hr^{-1} , and applying time to space calculations, a feature of 15 km spatial scale would affect a point for approximately 2 hours, which is in close agreement with the time-scale of the drying in Fig. 5 of around 2.5 hours. Thus it is entirely feasible that the vertical circulations associated with the easterly change generated this feature, and its amplitude was under-forecast due to the grid scale of the model. There are of course other possible reasons for the model failing to sufficiently resolve this feature, such as initial state error, inadequacies in the land surface scheme, inadequacies in the simulations of vertical mixing etc. However, it

would seem worthwhile to further investigate the circulations associated with these easterly changes at Canberra, given that Clarke (1983) shows that they are a common feature of the summertime climate in that region (although it might be questioned whether this change fits Clarke's "sea-breeze change" paradigm), and to provide some greater insight into the issues discussed earlier in this paragraph.

January 30 - synoptic overview

Figures 16, 17 and 18 show the mean-sea level pressure, upper-tropospheric height/wind, and screen level potential temperature and wind analyses at 0000 UTC 29 January through to 0600 UTC 30 January 2003. At the initial time (Fig. 16a) a surface trough oriented northwest/southeast lay along the coast from the Great Australian Bight to eastern Victoria, and a mid-latitude trough was over the Southern Ocean, with its axis around 130-132 E. A strong northwesterly jet stream can be seen in the upper troposphere associated with this deep, mid-latitude trough (Fig. 17a). While the surface trough along the southern Australian coast does not appear that significant, in combination with the coastal temperature gradient a strong convergence line extends right along the coast (Fig. 18a).

Between 0600 and 1200 UTC 29 January (Figs. 16b,c, 17b,c) the mid-latitude trough moved eastwards. During the daylight hours the coastal front intensified (Fig. 18b,c) and moved inland with the MSLP field showing more the pattern of a pre-frontal trough (Hanstrum et al 1990), with a closed low forming near the SA/Victoria border by 1200 UTC (Fig. 16c). Overnight the front moved eastwards, and by 1800 UTC 29 January (Fig. 18d) lay approximately from just west of Melbourne to Mildura. The surface manifestation of the mid-latitude trough is marked by the cyclonic curvature of the isobars (Fig. 16d) and of the winds (Fig. 18d) near the SA/Victoria border, and its westward slope with height is indicated by the fact that the 300 hPa flow is still northwesterly to the westward limit of the plotted area (132 E) (Fig. 17d), although the strengthening of the northwesterly isotach maximum perhaps suggests that the trough was amplifying. It should be noted that this approach of the cool change to central Victoria overnight does not match the paradigm of a late afternoon/early evening change at Melbourne that was first documented by Loewe

(1945), although the coastal temperature gradient was conjectured to be an intrinsic part of such systems.

By 0000 UTC 30 January the mid-latitude trough and the pre-frontal pressure troughs had “merged” (Fig. 16e) with a single wind change through NSW and northern Victoria near the eastern side of the strong temperature gradient (Fig. 18e). By 0600 UTC a low had formed on the trough line over southeastern NSW and a narrow coastal ridge had extended through Bass Strait (Fig. 16f), and a strong coastal front had developed along the southern side of the ranges in eastern Victoria: a strong wind discontinuity (Fig.18f) marked this change. Inland of the ranges the temperature gradient associated with the change was less strong and the associated wind change consequently more gradual. The 300 hPa trough (Fig. 17e,f) had continued to progress eastwards at some 4 degrees longitude (at 45 S) per 6 hours.

January 30 - observations and point forecasts

Clearly the change structure and evolution are complex in this case, particularly near the southeastern ranges, yet this is the most critical area for understanding the meteorology as it affected the Alpine fires that day. The time series of observations at 3 stations are shown (Fig. 19) – Mt. Hotham (elevation 1849 m) and representative of the most exposed parts of the elevated landscape, Wangaratta (elevation 156 m), representative of the plains north of the Great Dividing Range, and Gelantipy (elevation 755 m), on the southern slopes of the Great Dividing Range. At Mt Hotham (Fig. 19a,b), where the Forest Fire Danger Index (FFDI, Luke and McArthur 1978) reached nearly 50 on the afternoon of 30 January (Bureau of Meteorology 2003), it is seen that the wind speed (gust) increased steadily from around 20 (22) kn at 1300 UTC (midnight local daylight savings time) to 40 (>50) kn shortly after dawn, and maintained these speeds until around 0300 UTC when there was a lessening of the winds, but speeds (gusts) remained above 20 (40) kn until around 0930 UTC. The direction trace shows only a very slow backing of the wind from north through to northwest though this whole period, although if a particular time had to be placed on the arrival of a “cool change” the small backing of the wind at 0200 UTC, when the temperature began to fall (against the diurnal trend), the dewpoint rose, and the wind speed declined, is a defensible choice. However, the lack

of a significant, sustained direction shift makes this change hard to fit into many of the “cool change” conceptual models.

The time series of observations at Wangaratta (Fig. 19c,d), north of the divide, shows the characteristics of a nocturnal inversion between 1300 and 1900 UTC, with very low wind speeds and variable direction up to that time. However, after the breaking of the nocturnal inversion, the temperature increased rapidly, the dewpoint decreased with mixing of dryer air from aloft, and the wind speed also increased. Temperatures began to decline, dewpoints to increase, and the wind direction settled just south of west from around 0100 UTC (well before the climatological time of maximum temperature). Around that time, though, the winds increased to around 15 kn, with gusts above 20 kn for some hours. There was a further marked increase in wind speed and gustiness around 0800 UTC, when the temperature decreased by about 5K, although there is no direction shift with this “cool change”.

Gelantipy (Fig. 19e,f), south of the divide, shows an initial backing of the wind at around 0000 UTC, at which time the temperature ceased to rise, and with an increase in wind speed and gustiness. There is, however, a far more abrupt change between 0400 and 0430 UTC, with an abrupt wind change from northwest to southerly (preceded by a short increase in gustiness) and a marked cooling and moistening. It is unfortunate that a power outage led to a gap in the record shortly after that time, but this abrupt “cool change” marks the northward movement through Gelantipy of the thermal and wind gradient seen along the southern flanks of the ranges in Fig. 18e and in this case the timing of the wind change is unambiguous.

Figure 19 shows three quite different manifestations of a single synoptic-scale front/trough system, with the diabatic and topographic effects having different impacts depending on the detailed location and surrounding physiography of each station. Clearly no single conceptual model of a cool change arrival will suit these different locations, while the strong winds and gustiness at Mt. Hotham are a dramatic feature of the fire weather there.

January 30 – numerical predictions

Figure 20 shows the forecast meteograms from the operational 0.05° meso-LAPS Victorian domain NWP model for the same three stations as in Fig. 19. In all cases the forecast time series are rather smoother than the observation time-series; however, most of the broad features of the observations are seen in the forecasts, and perhaps more importantly, the different change structures at the three stations are well represented in the forecasts. The abrupt change at Gelantipy, with a marked cooling and moistening, preceded by a period of enhanced gustiness is well forecast. At Wangaratta the forecast drying following the breaking of the nocturnal inversion is only weakly represented, but its timing is well forecast. The temperature time-series is well represented, with a maximum earlier than the climatological mean time, and a more rapid cooling later in the afternoon, and more particularly, the “double maximum” in gustiness is extremely well forecast. At Mt Hotham, the average wind speed is under-forecast, however the strong and persistent period of gustiness, the very slow backing of the winds, and timing of the commencement of increasing dewpoints (~0100 UTC) and of decreasing temperatures (~0330 UTC) are reasonably well forecast.

In plan view the 0.05° meso-LAPS forecasts of screen-level potential temperature (overlaid with near-surface wind barbs) and forecast wind gusts are shown at 1800 UTC 29 January, and 0000 and 0600 UTC 30 January 2003 (18, 24 and 30-hour forecasts) in Fig. 21. At 1800 UTC (Fig. 21a,b) the cool change is east of Melbourne, wind speeds over the Alps are up to 15 kn, and gusts to 30 kn are forecast (Fig. 21b). By 0000 UTC (Fig. 21c,d) there is an almost east-west change line from north of Melbourne to east Gippsland, with the change having surged along the coast. The strongest temperature gradients are along the eastern coastline of Victoria, where the change had most recently crossed the coast. North of the ranges the northwesterly winds are seen to be backing towards the west, and the isotherms decreasing in value slowly to the west suggest weak adiabatic cool advection there. The gust forecast (Fig. 21d), though, shows a dramatic change from that at 1800 UTC, with gusts over 50 kn forecast widely over the Alpine areas. By 0600 UTC (Fig. 21e,f) the cooler air had moved northward along the southern side of the Alps as the deeper layer of cool air developed, and an abrupt convergence line is seen in eastern Victoria (cf the Gelantipy observations, Fig.19). Cooler air has slowly advanced north of the ranges and the winds have backed and strengthened there with gusts to 35 kn forecast (cf the

period of late wind increase at Wangaratta seen in Fig. 19), while the strongest gusts over the Alps have moved to the northeast.

January 30 - diagnosis

The comparison of the forecasts and the observed conditions on January 30 shows that the mesoscale NWP model performed with a very high degree of skill. Given this, the model forecast fields can be used to diagnose the processes operating on that day. The primary feature of the day was the extremely strong and gusty winds that occurred over the Alpine areas from early on January 30, however the difference between the frontal structures observed north and south of the ranges is also of interest.

First, given that the gust at the surface has been associated with the highest wind speed in the mixed layer, which, on January 30, extended from the surface to around 800 hPa over northern and eastern Victoria at 0000 UTC, the 800 hPa temperature and wind speed fields at 1200 UTC and 1800 UTC 29 January, and at 0000 UTC 30 January are shown in Fig. 22, while Fig. 23 shows vertical cross-sections along the line shown in Fig. 22. At 1200 UTC (Fig. 22a) two zones of strong temperature gradient can be identified, one concentrated over the SA gulfs, and a second over Bight waters. These can be interpreted as a coastal front and a deep mid-latitude front respectively. The differing vertical structures of these fronts can be seen in the cross section (Fig. 23a), with the coastal front showing near vertical isentropes to around 600 hPa, while the mid-latitude front has sloping isentropes extending through a considerable depth of the troposphere (note that while the cross-section shown in Fig. 23a does not intersect the mid-latitude front at 800hPa, the isentropes in the southwest of the section in Fig. 23a show the clear sloping structure of this front extending to the surface). Lower tropospheric isotach maxima were associated with each of these baroclinic zones. By 1800 UTC the temperature gradient associated with the coastal front had strengthened over Victoria (Fig. 22b), and both systems were moving eastwards, although the southern system was advancing more rapidly. With the developing temperature gradient, a weakly-defined isotach maximum had developed over northern Victoria. The cross-section at 1800 UTC 29 January (Fig. 23b) shows a strengthening of the thermal gradient in the lower troposphere near the

middle of the section, suggesting that frontogenesis is occurring above the boundary layer in this feature that was associated above with the inland movement of the coastal front, but a surface nocturnal inversion is seen below this lower tropospheric front. The component of the ageostrophic flow in the plane of the cross-section and the vertical motion fields at 1800 UTC (Fig. 24), is qualitatively consistent with the direct cross-frontal ageostrophic circulations that would be diagnosed by the Sawyer-Eliassen equation (eg Bluestein, 1986) during frontogenesis. These ageostrophic wind vectors are directed to the southwest, and thus indicate that the northwesterly low-level pre-frontal jet (Fig. 22) is being accelerated. With the development of a nocturnal surface inversion, this acceleration of the air parcels in response to the increasing temperature gradient is not inhibited by surface friction. Accordingly this frontogenesis above the nocturnal inversion led to the development of a strengthened pre-frontal low-level jet, which by 0000 UTC 30 January exceeded 25 m s^{-1} over the eastern Victorian mountains (Fig. 22c) as this process continued while the systems move eastwards. The cross-section at 0000 UTC 30 January (Fig. 23c) shows that daytime heating had by that time eroded the nocturnal surface inversion, leaving a mixed layer from the surface to around 800 hPa, and thus allowing this low-level jet to reach the surface as gusts via thermal and mechanical mixing. Thus while frontogenesis above a nocturnal surface inversion allowed the acceleration of a pre-frontal low-level jet, the erosion of the same nocturnal inversion after sunrise allowed this strengthened low-level jet to be realised as enhanced surface speed and gustiness over the elevated terrain of southeastern Australia.

Figure 18 e,f and Fig. 21 showed that the cool change moved across northern Victoria as a slow backing of the wind, rather than as a sharp wind-shift, and that cooler southwesterlies did not become fully established at, for example, Wangaratta (see Fig. 19) until the early evening. However, Hewson's model of the cold-frontal location applied to Fig. 18f would place the cold front well east of Wangaratta in the mid afternoon, although only if the criterion requiring that the thermal gradient be of "sufficient" strength is relaxed somewhat from that which might be applied to the front south of the ranges. Further, the temperature gradient does appear to intensify in the early evening with the onset of the strengthening southwesterly winds.

From the thermodynamic equation, local temperature changes result from advection and diabatic processes. The local change can be calculated from successive model outputs, in this case hourly, and advection can be calculated from model fields, allowing the diabatic heating rate to be calculated as a residual. Applying this process to hourly model output, and displaying the results (Fig. 25) along the line shown in Fig. 18, selected to be approximately normal to the isentropes, it is seen that during the daytime on January 30, the diabatic heating rate increased with distance west of the front. Thus, while temperatures decrease with distance west of the front, the gradient in diabatic heating was acting to reduce the temperature gradient in the frontal zone – the diabatic heating was frontolytic. Deslandes et al (1999) also show the frontolytic effect of daytime diabatic heating in the post-frontal boundary layer. Figure 26 shows the vertical temperature cross-section along the same line used in the diagnosis of diabatic heating rate. The nose of the front is clearly seen, with vertically oriented isentropes close to the ground, indicating a mixed layer extending over some depth in the post-frontal air. However, the depth of this post-frontal mixed layer decreases to the west. If a very simple assumption of constant sensible heat flux along this section is made, and that the surface sensible heat flux will be distributed evenly through the mixed layer, then the deeper the post-frontal mixed layer, then the less the temperature increase through the depth of that mixed layer, consistent with the profile in Fig. 24. The greater depth of the post-frontal mixed layer immediately following the frontal passage might be explained conceptually if it is considered that a post-frontal air parcel further east has had a longer period over land than one further to the west, and so has had more time to be modified by diabatic heating. (It should be noted that Reeder and Tory (2005) show a similar vertical structure in their idealised modelling study, but argue that the structure is generated by horizontal variations in sensible heat flux.) The net result of these processes, though, is that diabatic processes act to weaken the cold front, and as a consequence the rate of backing of the winds, through northern Victoria during the daylight hours. Once the sensible heating weakens as the afternoon advances, this effect becomes less evident, broad-scale frontogenetic processes become dominant again, the temperature gradient increases, the winds back more sharply, and cool advection west of the front becomes stronger, consistent with the observations at Wangaratta (Fig. 19).

Discussion

Two days on which the weather-influenced fire danger reached extreme levels over southeastern Australia, and on which extreme fire behaviour occurred, have been described in some detail. On each day cold fronts, or cool changes, were crossing southeastern Australia, and it was shown that diabatic processes had a profound effect on the structure and evolution of these cool changes, leading to wide geographical differences in the wind and temperature realised at different locations during the passage of a single cool change. Based on these two case studies, both overnight frontogenesis above the surface inversion, and daytime frontolysis due to diabatic heating gradients are processes that need to be considered in addition to the range of other conceptual models of cool change structure over southeastern Australia that have been published during the last 25 years. These processes should not, though, be seen as new conceptual models, but rather a reinforcement of the concept that a range of processes can modulate the structure of a cool change, depending on its location relative to the coastal or topographic gradients and to the phase of the diurnal heating cycle.

On each of the days discussed in this paper the very strong and gusty winds that contributed to the severity of the fire weather on the ground were associated with sub-synoptic or mesoscale isotach maxima near the top of the mixed layer of the troposphere, which in these cases was 2000-4000 m deep. On those days the operational mesoscale nwp models resolved these features, and using simple diagnostic techniques can provide highly instructive forecast guidance that is not available from more traditional, surface based, forecast products.

The drying episodes at Canberra late on the afternoon of 18 January are interesting features, and both Werth and Ochoa (1993) and Charney et al (2003) have shown other examples where mesoscale drying events can be associated with enhanced fire activity by assisting the drying of fine fuels. It was hypothesised that there were two identifiable periods of successive reduction in near-surface humidity, and that these could be associated with separate mesoscale circulation systems. The first was the passage of a mid-tropospheric humidity minimum that could be clearly identified and tracked in the satellite imagery over southern NSW and the ACT, with

surface dryings observed as the “dry slot” in the water-vapour imagery moved overhead. Mid-tropospheric dry slots visible in the water-vapour imagery are likely to be identifiable relatively easily, and future effort will be devoted to understanding their relation to surface drying events, as monitoring of such features appears to have immediate potential as part of the fire weather forecasting process.

The hypothesis was advanced in this paper that the second drying period at Canberra, just before the easterly change arrived, was associated with the vertical circulation of the easterly change, although no physical evidence for this hypothesis was presented. Given that easterly changes are a relatively common feature of Canberra’s summertime climate (Clarke, 1983), further investigation of the mesoscale structure of these changes, and the predictability of these structures, is warranted.

The lower mid-tropospheric wet-bulb potential temperatures associated with regions that can be identified as “dry slots” in the water vapour imagery has been associated with convective destabilisation of the atmosphere (Browning 1994). It is perhaps not a coincidence, therefore, that a huge pyrocumulus cloud was observed above the Canberra fire on the afternoon of January 18, and later that day thunderstorms occurred off the NSW coast on the eastern end of the dark band in the water vapour imagery (Fig. 10 c,d). More active, or “unpredictable” fire behaviour has been noted in conditions of decreased atmospheric stability, and attempts to forecast this using techniques such as the Haines Index (Werth and Ochoa 1993) have been developed. However, the Haines Index is less useful as a discriminant of such conditions when the mixed layer depth is regularly deep (Werth and Werth 1998) and these are just the conditions that are observed over southeastern Australia inland from the coastal regions during the summer. However, the known association between mid-tropospheric dry slots and reduced atmospheric stability may make the water vapour imagery a useful guide to areas where the atmospheric stability over an active fire may be reduced, in addition their effects on lower-atmospheric drying already discussed.

McLeod (2003) reported the hypothesis that the gustiness and drying observed at Canberra Airport on the afternoon of 18 January was due to vertical circulations associated with the fire-induced pyrocumulus cloud observed that afternoon. In this

paper it has been argued that the gustiness and drying observed at Canberra Airport was due to sub-synoptic scale circulation systems that were coherent in time and space over several hours and several hundred kilometres. This is not to say, however, that small-scale, intense atmospheric flows did not occur close to the fire as a result of fire-atmosphere interactions, and anecdotal reports and post-event damage surveys indicate that such circulations did occur on 18 January. However, these are on a scale much smaller than the mesoscale circulation features described in this paper, and it is reasonable to speculate that the enhanced fire activity driven by the larger-scale circulations described in this paper may indeed have made these small scale, intense fire-atmosphere interactions more likely.

Acknowledgements

The author has received assistance from many people in the preparation of this manuscript. Hank de Wit's magnificent data recovery and plotting package generated Figure 8. Manuela Burgers assisted in my understanding the scaling of the surface wind stresses in the model output that was necessary in order to calculate the gustiness plots. Anton Beljaars and Dale Hess provided the gust diagnosis code. Peter Steinle corrected the moisture analysis "bug" that enabled the hindcast for the Canberra case to be computed with more realistic moisture fields, while Noel Davidson, Kevin Tory, and Robin Bowen provided the scripts that were used to reassimilate the data for that forecast. The presentation of the paper has been improved by the constructive comments of Dale Hess, Tony Bannister, and Frank Woodcock. I'm grateful to all these people for their generous sharing of their time and knowledge.

References

- Beljaars, A.C.M., 1987. The influence of sampling and filtering on measured wind gusts. *J. Atmos. Oceanic Technol.* 4, 613-626.
- Bluestein, H.B. 1986. Fronts and jet streaks: A theoretical perspective. *Mesoscale Meteorology and Forecasting*. P.S.Ray, Ed. Amer. Met. Soc., 793pp.
- Brasseur, O., 2001. Development and application of a physical approach to estimating wind gusts. *Mon. Wea. Rev.* 129, 5-25.
- Browning, K.A., 1994. Airflow and structure of precipitation systems in extratropical cyclones. Proceedings of an international symposium "The life cycles of extratropical cyclones", Bergen 1994. Gronas, S and Shapiro, M.A., eds.
- Bureau of Meteorology, 2003. Meteorological aspects of the eastern Victorian fires January-March 2003. Bureau of Meteorology, Victoria. 82pp
- Charney, J.J., Bian, X., Potter, B.E., and Heilman, W.E., 2003. The role of a stratospheric intrusion in the evolution of the Double Trouble State Park wildfire. *5th Symposium on Fire and Forest Meteorology and 2nd International Wildland Fire Ecology and Fire Management Congress*. November 16-29, 2003. Orlando, Florida. American Meteorological Society.
- Clarke, R.H., 1983. Fair weather nocturnal inland wind surges and atmospheric bores: Part I Nocturnal wind surges. *Aust. Meteor. Mag.* 31, 133-145.
- Colquhoun, J.R., Shepherd, D.J., Coulman, C.E., Smith, R.K., and McInnes, K., 1985. The southerly burster of south eastern Australia: an orographically forced cold front. *Mon. Wea. Rev.* 113, 2090-2107.
- Deslandes, R., M.J.Reeder, and G.A.Mills, 1999: A synoptic study of fronts using RASP analyses for the central Australian fronts experiment - nocturnal frontogenesis. *Aust. Meteor. Mag.* 48, 87-110.

- Hanstrum, B.N., Wilson, K.J., and Barrell, S.L. 1990. Pre-frontal troughs over southern Australia. Part I: A climatology. *Wea. And Forecasting* 5, 22-31.
- Hewson, T.D. 1998. Objective fronts. *Meteorol. Appl.* 5, 37-65.
- Lowe, F. 1945. Frontal hours at Melbourne. *R.A.A.F. Weather research and Development Bulletin*, 3, 13-9.
- Luke, R.H., and McArthur, A.G., 1978. Bushfires in Australia. Australian Government Publishing Service, Canberra, Australia. 359pp.
- McLeod, R.N. 2003. Inquiry into the operational response to the January 2003 bushfires in the ACT. Department of Urban Services, ACT. 273pp.
- Mills, G.A., 2002. A case of coastal interaction with a cool change. *Aust. Meteor. Mag.* 51, 203-221.
- Mills, G.A., 2005. A re-examination of the synoptic and mesoscale meteorology of Ash Wednesday 1983. *Aust. Meteor. Mag.* 54, 35-55.
- Mills, G.A. and Pendlebury, S., 2003. Processes leading to a severe wind-shear incident at Hobart Airport. *Aust. Meteor. Mag.* 52, 171-188.
- Morgan, E.J., 2002. Wind change forecast accuracy in Victoria during the 1996-7 to 2000-1 fire seasons. Extended abstracts, 2002 Weather Services Scientific Conference, 66-67. Bureau of Meteorology, Box1289K, Melbourne, Australia. 117pp.
- Puri, K., Dietachmeyer, G.D., Mills, G.A., Davidson, N.E., Bowen, R.A., and Logan, L.W. 1998. The new BMRC Limited Area Prediction System. LAPS. *Aust. Met. Mag.* 47, 203-23.

Reeder, M.J., and Tory, K., 2005. The effect of the continental boundary layer on the dynamics of fronts in a two-dimensional model of baroclinic instability. Part II. Surface heating and cooling. *Quart. J. Roy. Meteor. Soc.* In Press.

Verkaik, J.W., 2000. Evaluation of two gustiness models for exposure correction calculations. *J. Appl. Meteor.* 37, 461-469.

Weiringa, J., 1986. Roughness-dependent geographical interpolation of surface wind speed averages. *Quart. J. Roy. Meteor. Soc.* 112, 867-889.

Weldon, R.B., and Holmes, S.J. 1991. Water Vapour imagery. Interpretation and applications to weather analysis and forecasting. *NOAA Technical Report NESDIS 57*. National Oceanic and Atmospheric Administration, Washington, D.C., 213pp.

Werth, P., and Ochoa, R. 1993. The evaluation of Idaho wildfire growth using the Haines Index. *Wea. And Forecasting* 8, 223-234.

Werth, J., and Werth, P., 1998. Haines Index climatology for the western United States. *Fire Management Notes* 58, 8-17.

Captions to figures

Figure 1. Upper panel – Locality map of the southeastern part of Australia, with place-names referred to in the text. Middle panel – Map of eastern Victoria and southeastern NSW showing locations of observing stations used in the paper – Goulburn (YGLB), Canberra (YSCB), Cabramurra (CBMR), Cooma (YCOM), Thredbo (THDB), Wangaratta (YWGT), Mt. Hotham (HOTH), and Gelantipy (GELA). The station location is at the top left-hand corner of the first letter of each acronym. Lower panel – topography (m) used in the operational 0.05° meso-LAPS model. Contour intervals at 100, 250, 500, 750, 1000, and 1250m.

Figure 2. LAPS mean-sea-level pressure analyses from 0600 UTC 17 January to 1200 UTC 18 January 2003. Contour interval 2 hPa.

Figure 3. LAPS 300 hPa height/isotach analyses at 0000 UTC 18 January 2003. Geopotential height (heavy contours) at 60 gpm intervals, and isotachs (light contours) are shaded above 20 m s^{-1} (light) and 40 m s^{-1} (dark).

Figure 4. LAPS screen-level potential temperature and low-level wind speed analyses at 6-hour intervals from 0600 UTC 17 January to 1200 UTC 18 January 2003. Contour interval for potential temperature is 2K, while the wind barbs have their usual meteorological meaning.

Figure 5. Time series of observations from Canberra Airport (YSCB, see Fig. 1) from 1300 UTC 17 January 2003 to 1200 UTC 18 January 2003. Upper panel – wind direction (degrees) in black, with wind speed and gust (knots) in red and green respectively. Lower panel – temperature (red) and dewpoint (green), both in C. Note the offset scales on the ordinates of the lower panel.

Figure 6(a). Time series of observations from Thredbo (THDB, see Fig. 1) and Cooma (YCOM) from 1300 UTC 17 January 2003 to 1200 UTC 18 January 2003. Upper panel – wind direction (degrees) in black, with wind speed and gust (knots) in red and green respectively. Lower panel – temperature (red) and dewpoint (green), both in C. Note the offset scales on the ordinates of the lower panels.

Figure 6(b). Time series of observations from Cabramurra (CBMR, see Fig. 1) and Goulburn (YGLB) from 1300 UTC 17 January 2003 to 1200 UTC 18 January 2003. Upper panel – wind direction (degrees) in black, with wind speed and gust (knots) in red and green respectively. Lower panel – temperature (red) and dewpoint (green), both in C. Note the offset scales on the ordinates of the lower panels.

Figure 7. Time series of forecast parameters interpolated at hourly intervals from the Sydney-region meso-LAPS model at the location of Canberra Airport (YSCB, see Fig. 1) from 1300 UTC 17 January 2003 to 1200 UTC 18 January 2003. Upper panel – wind direction (degrees) in black, with wind speed and gust (knots) in red and green respectively. Lower panel – temperature (red) and dewpoint (green), both in C. Note the offset scales on the ordinates of the lower panel.

Figure 8. Upper-air sounding at Wagga for the flight at 0000 UTC 18 January 2003

Figure 9. 700 hPa temperature and wind speed at 3-hourly intervals from the 0.125° meso-LAPS model, valid at 2100 UTC 17 January, and 0000, 0300, and 0600 UTC 18 January 2003. Temperature contours are dashed, at 1K intervals, while isotachs (heavy contours) are at 10, 15, and 20 m s⁻¹, with areas greater than 15 m s⁻¹ shaded.

Figure 10. Enhanced Water-Vapour channel (6-7 μm) imagery from the GMS-5 satellite at 2330 UTC 17 January, and 0230, 0430, and 0530 UTC 18 January. The line in the upper panel marks the location of the cross-section in Fig. 11.

Figure 11. Mixing ratio cross section from the 0.125° meso-LAPS 12-hour forecast based at 1200 UTC 17 January 2003. Contour interval 1 gm Kg⁻¹.

Figure 12. Time series of observations from Wagga (Fig. 1) from 1300 UTC 17 January 2003 to 1200 UTC 18 January 2003. Temperature (red) and dewpoint (green), both in C. Note the offset scales on the ordinates of the lower panel.

Figure 13. 0.05° meso-LAPS forecast of screen-level potential temperature and wind speed valid 0500 UTC 18 January 2003. The line marks the position of the vertical cross-sections shown in Fig.11, and the arrow indicates the location of Canberra.

Figure 14. 0.05° meso-LAPS forecast of screen-level dewpoint (C) valid 0500 UTC 18 January 2003.

Figure 15. Cross-sections along the line in Fig.10. Upper panel shows potential temperature (solid, contour interval 2K) and wind speed (dashed, contour interval 5 ms^{-1}), middle panel vertical motion (hPa hr^{-1} , negative contours dashed), and lower panel mixing ratio (gm Kg^{-1}).

Figure 16. LAPS mean-sea-level pressure analyses from 0000 UTC 29 January to 0600 UTC 30 January 2003. Contour interval 2 hPa.

Figure 17. LAPS 300 hPa height/isotach analyses from 0000 UTC 29 January to 0600 UTC 30 January 2003. Geopotential height (heavy contours) at 60 gpm intervals, and isotachs (light contours) are shaded above 30 m s^{-1} (light) and 60 m s^{-1} (dark).

Figure 18. LAPS screen-level potential temperature and low-level wind speed analyses at 6-hour intervals from 0000 UTC 29 January to 0600 UTC 30 January 2003. Contour interval for potential temperature is 2K, while the wind barbs have their usual meteorological meaning. The line in the lower panel shows the locations of diagnostics and cross-sections in Figs. 25 and 26.

Figure 19. Time series of observations from Wangaratta (YWGT, see Fig. 1), Mt. Hotham (HOTH) and Gelantipy (GELA) from 1300 UTC 29 January 2003 to 1200 UTC 30 January 2003. Left panels – wind direction (degrees) in black, with wind speed and gust (knots) in red and green respectively. Right panels – temperature (red) and dewpoint (green), both in C. Note the offset scales on the ordinates of the right-hand panels.

Figure 20. Time series of Melbourne-region 0.05° Meso-LAPS forecasts for Wangaratta (YWGT, see Fig. 1), Mt. Hotham (HOTH) and Gelantipy (GELA) from

1300 UTC 29 January 2003 to 1200 UTC 30 January 2003. Left panels – wind direction (degrees) in black, with wind speed and gust (knots) in red and green respectively. Right panels – temperature (red) and dewpoint (green), both in C. Note the offset scales on the ordinates of the right-hand panels.

Figure 21. Screen-level potential temperature (contour interval 2K) overlaid with near-surface wind barbs (left column), and forecast surface wind gust (right column) for 18, 24 and 30-hour forecasts from the 0.05° meso-LAPS model run valid at 1800 UTC 29 January (top row), 0000 UTC (middle row) and 0600 UTC (bottom row) 30 January 2003.

Figure 22. Forecast 800 hPa temperature and wind speed at 6-hourly intervals from the 0.125° meso-LAPS model, valid at 1800 UTC 29 January, and 0000 and 0600 UTC 30 January 2003. Temperature contours are at 1K intervals, while isotachs are shaded above 15 m s⁻¹ (light) and 20 m s⁻¹ (darker). The dark line in the upper panel shows the position of the cross-sections in Fig. 23.

Figure 23. Cross-sections along the line shown in Fig. 22, valid at 1200 and 1800 UTC 29 January, and 0000 UTC 30 January 2003. Potential temperature (black) is contoured at 2K intervals, with wind speed (dashed red) at 5 m s⁻¹ intervals.

Figure 24. Cross-section, along the line shown in Fig. 22, valid at 1800 UTC 29 January, of the component of the ageostrophic wind vector in the plane of the section, with vertical motion (hPa/hr, negative values dashed) contoured.

Figure 25. Upper panel – profile of forecast 950 hPa screen-level potential temperature at 0400 UTC 30 January 2003 along the line shown in Fig. 18. Lower panel is the profile of the diabatic heating rate (K hr⁻¹) diagnosed from the forecast valid at 0300 and 0400 UTC along the same section.

Figure 26. Cross-section of forecast potential temperature (solid contours, K) and wind speed (dashed contours, m s⁻¹) along the line of the section shown in Fig.18.

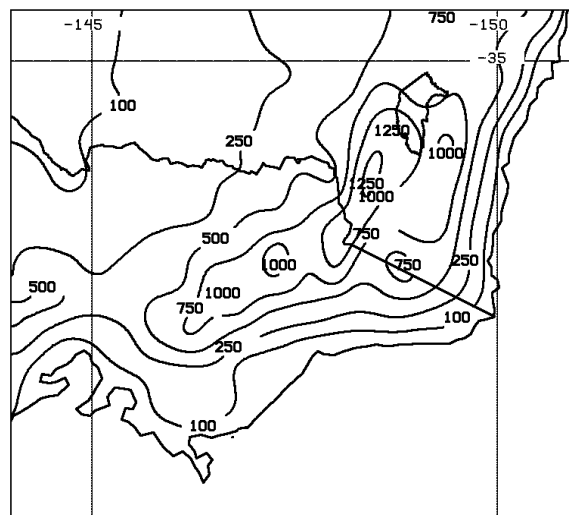
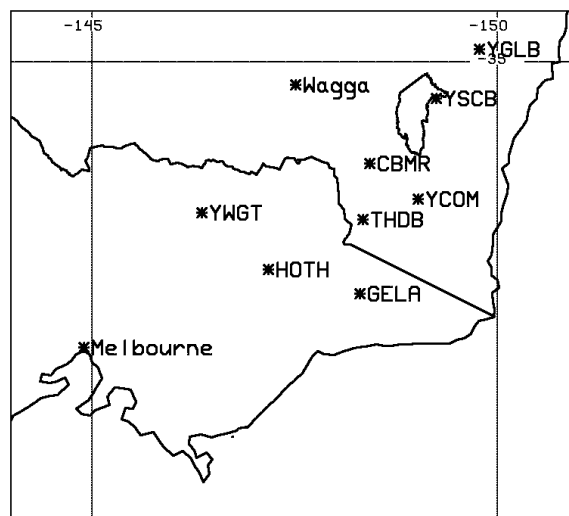
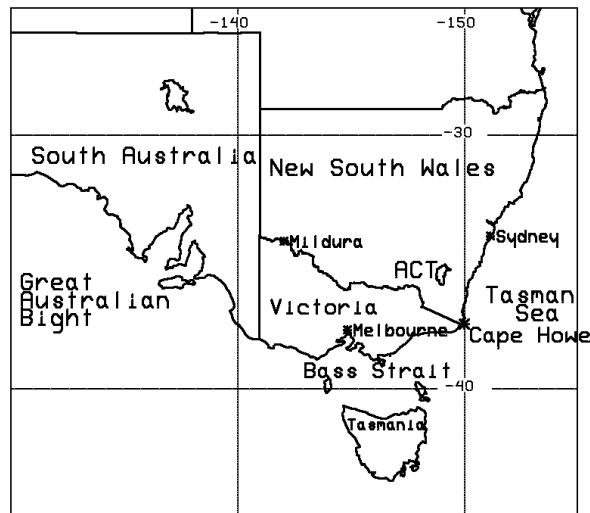


Figure 1. Upper panel – Locality map of the southeastern part of Australia, with place-names referred to in the text. Middle panel – Map of eastern Victoria and southeastern NSW showing locations of observing stations used in the paper – Goulburn (YGLB), Canberra (YSCB), Cabramurra (CBMR), Cooma (YCOM), Thredbo (THDB), Wangaratta (YWGT), Mt. Hotham (HOTH), and Gelantipy (GELA). The station location is at the top left-hand corner of the first letter of each acronym. Lower panel – topography (m) used in the operational 0.05° meso-LAPS model. Contour intervals at 100, 250, 500, 750, 1000, and 1250m.

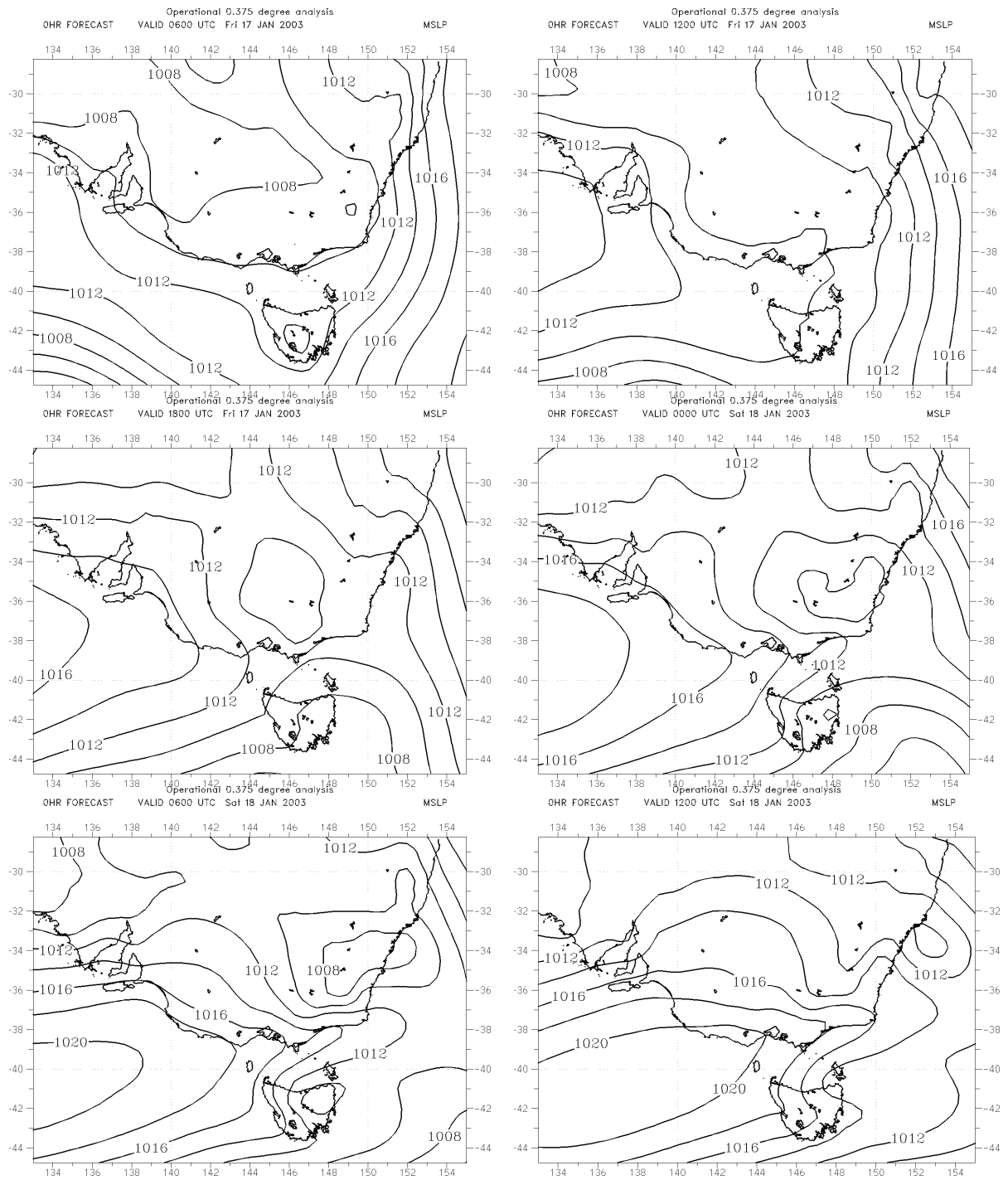


Figure 2. LAPS mean-sea-level pressure analyses from 0600 UTC 17 January to 1200 UTC 18 January 2003. Contour interval 2 hPa.

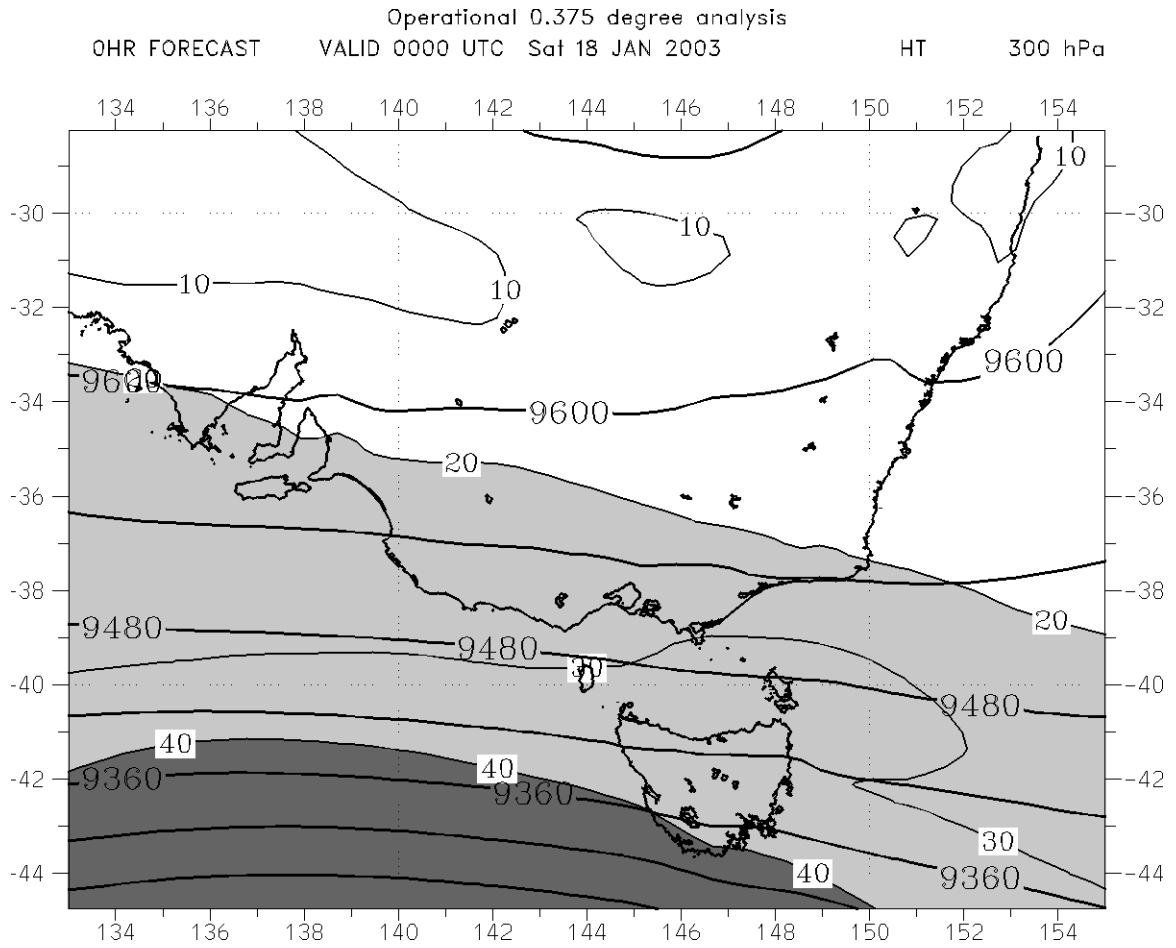


Figure 3. LAPS 300 hPa height/isotach analyses at 0000 UTC 18 January 2003. Geopotential height (heavy contours) at 60 gpm intervals, and isotachs (light contours) are shaded above 20 m s^{-1} (light) and 40 m s^{-1} (dark).

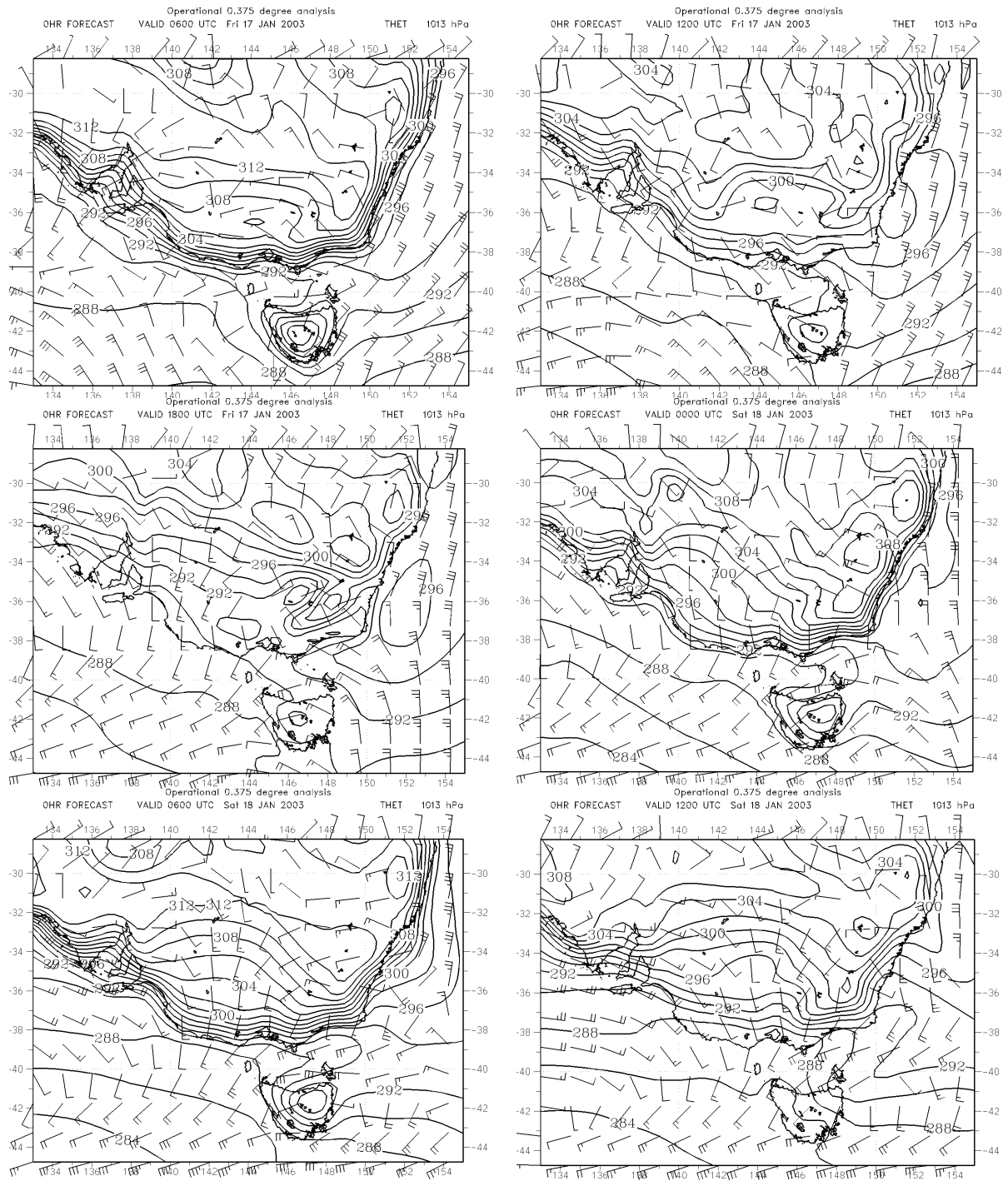


Figure 4. LAPS screen-level potential temperature and low-level wind speed analyses at 6-hour intervals from 0600 UTC 17 January to 1200 UTC 18 January 2003. Contour interval for potential temperature is 2K, while the wind barbs have their usual meteorological meaning.

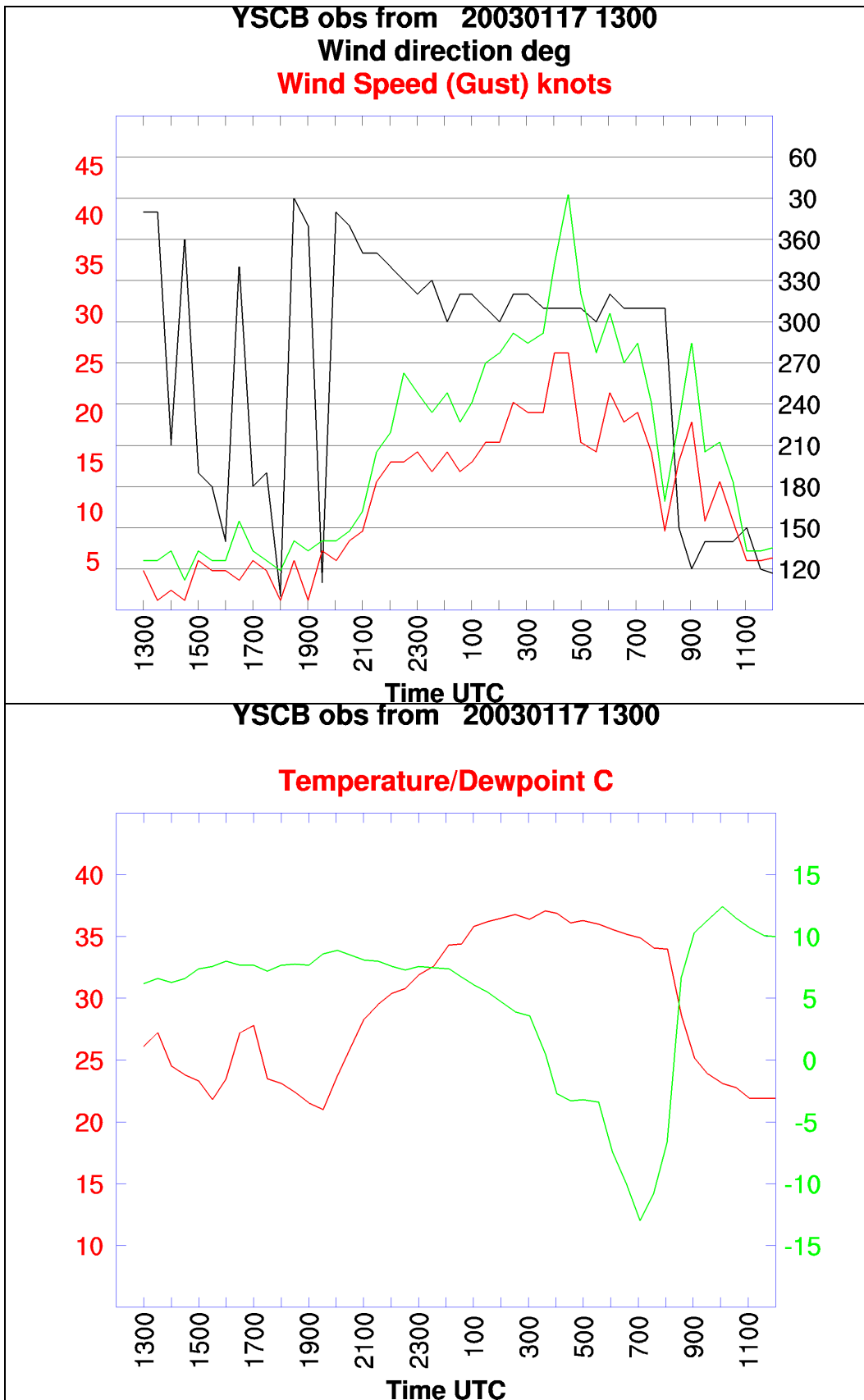


Figure 5. Time series of observations from Canberra Airport (YSCB, see Fig. 1) from 1300 UTC 17 January 2003 to 1200 UTC 18 January 2003. Upper panel – wind direction (degrees) in black, with wind speed and gust (knots) in red and green respectively. Lower panel – temperature (red) and dewpoint (green), both in C. Note the offset scales on the ordinates of the lower panel.

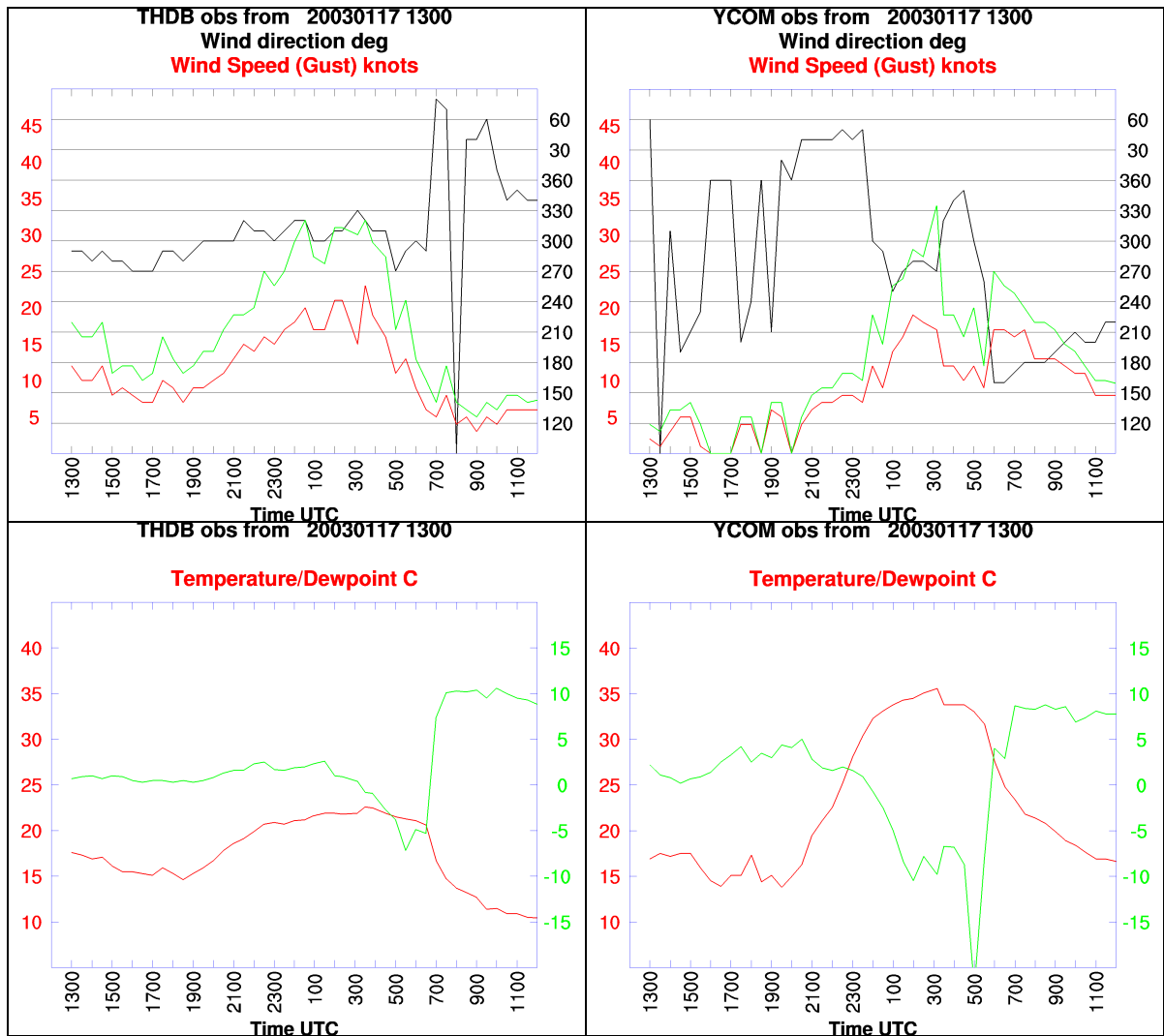


Figure 6(a). Time series of observations from Thredbo (THDB, see Fig. 1) and Cooma (YCOM) from 1300 UTC 17 January 2003 to 1200 UTC 18 January 2003. Upper panel – wind direction (degrees) in black, with wind speed and gust (knots) in red and green respectively. Lower panel – temperature (red) and dewpoint (green), both in C. Note the offset scales on the ordinates of the lower panels.

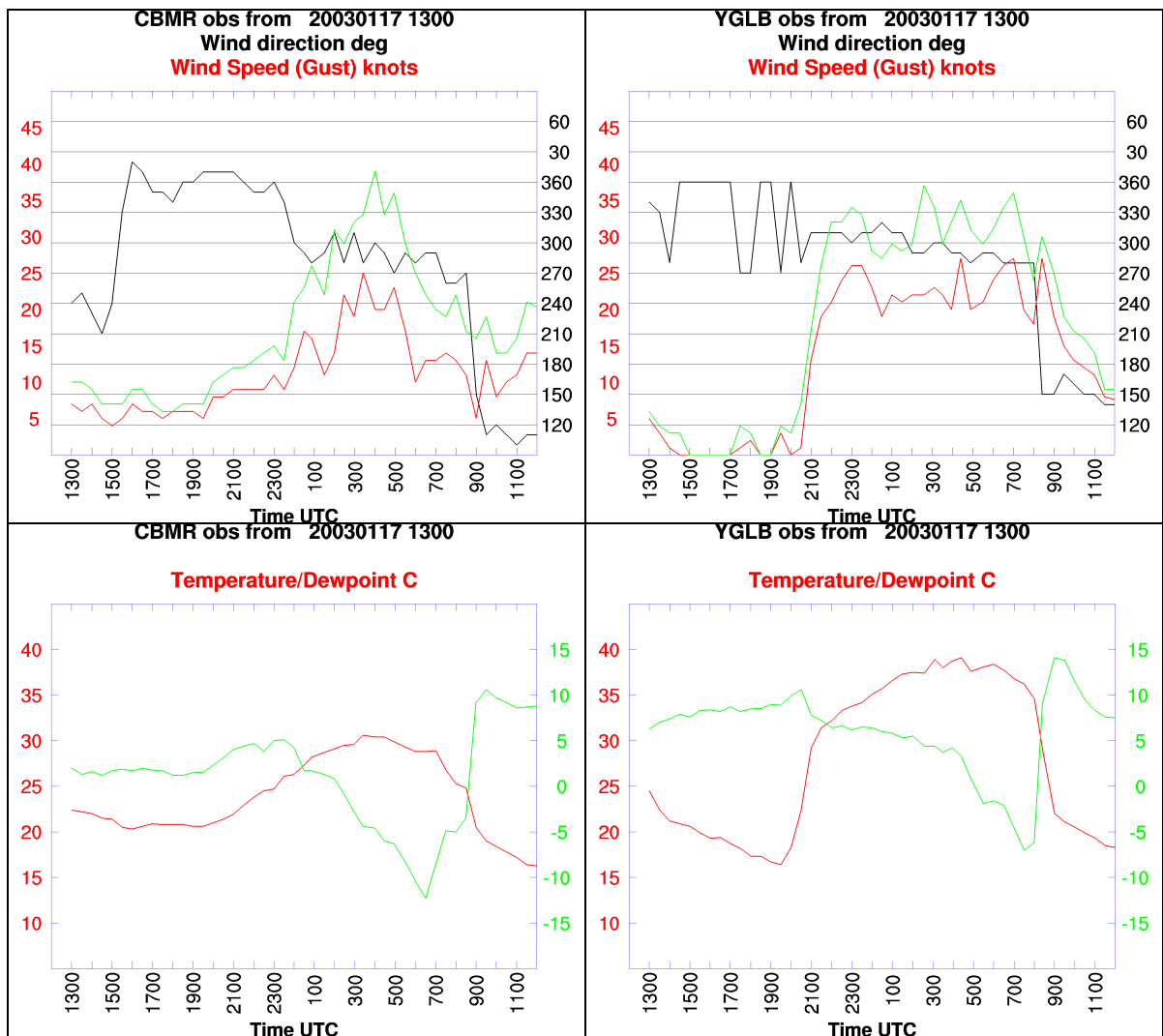


Figure 6(b). Time series of observations from Cabramurra (CBMR, see Fig. 1) and Goulburn (YGLB) from 1300 UTC 17 January 2003 to 1200 UTC 18 January 2003. Upper panel – wind direction (degrees) in black, with wind speed and gust (knots) in red and green respectively. Lower panel – temperature (red) and dewpoint (green), both in C. Note the offset scales on the ordinates of the lower panels.

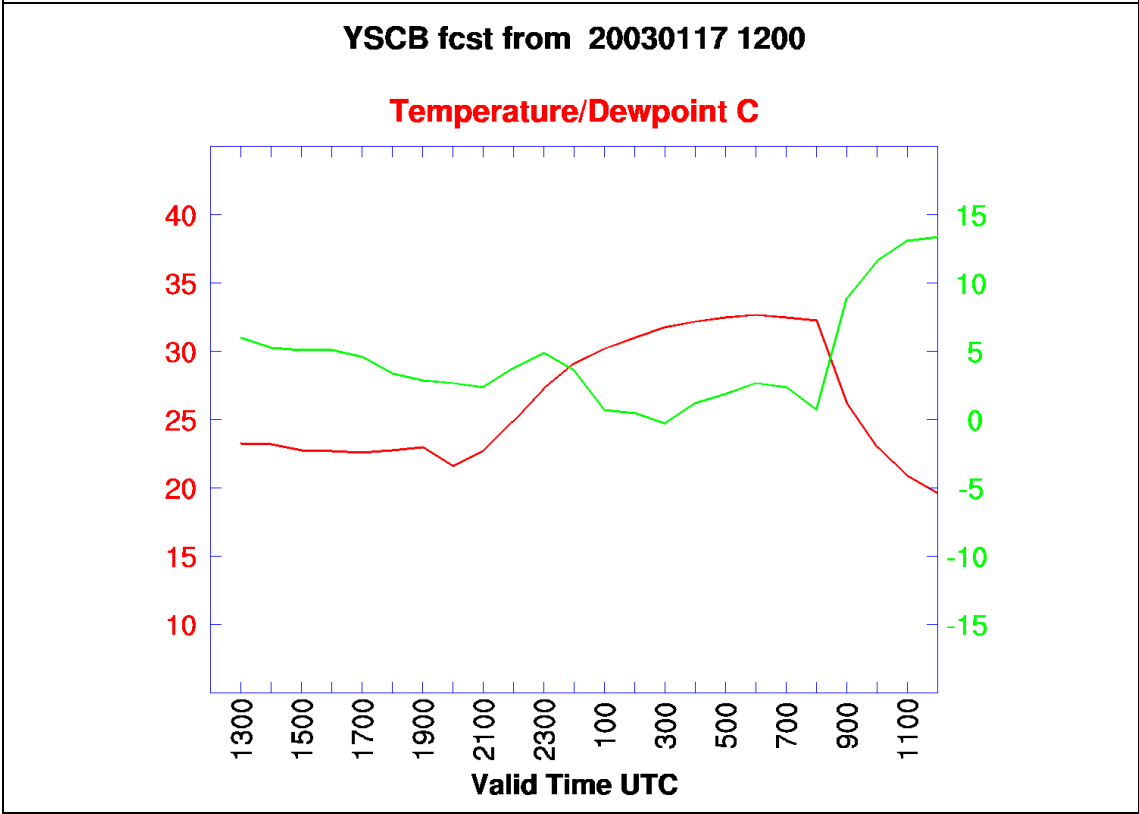
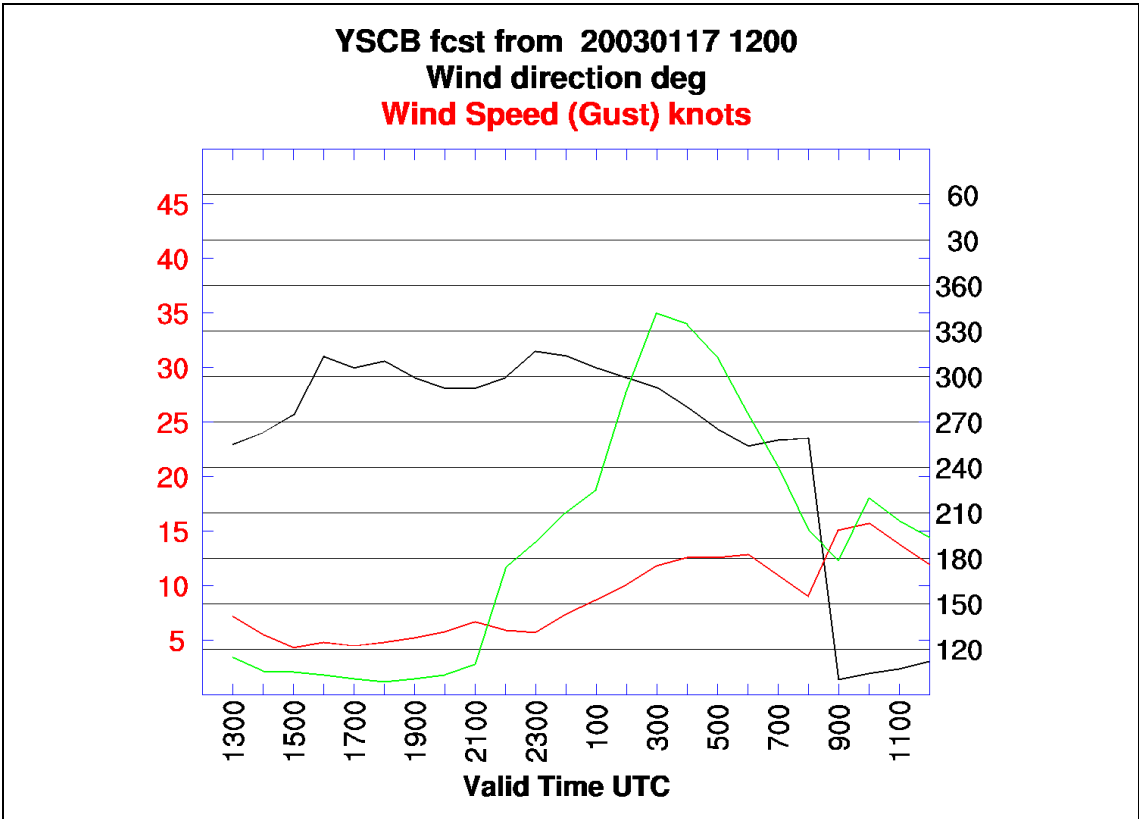


Figure 7 Time series of forecast parameters interpolated at hourly intervals from the Sydney-region meso-LAPS model at the location of Canberra Airport (YSCB, see Fig. 1) from 1300 UTC 17 January 2003 to 1200 UTC 18 January 2003. Upper panel – wind direction (degrees) in black, with wind speed and gust (knots) in red and green respectively. Lower panel – temperature (red) and dewpoint (green), both in C. Note the offset scales on the ordinates of the lower panel.

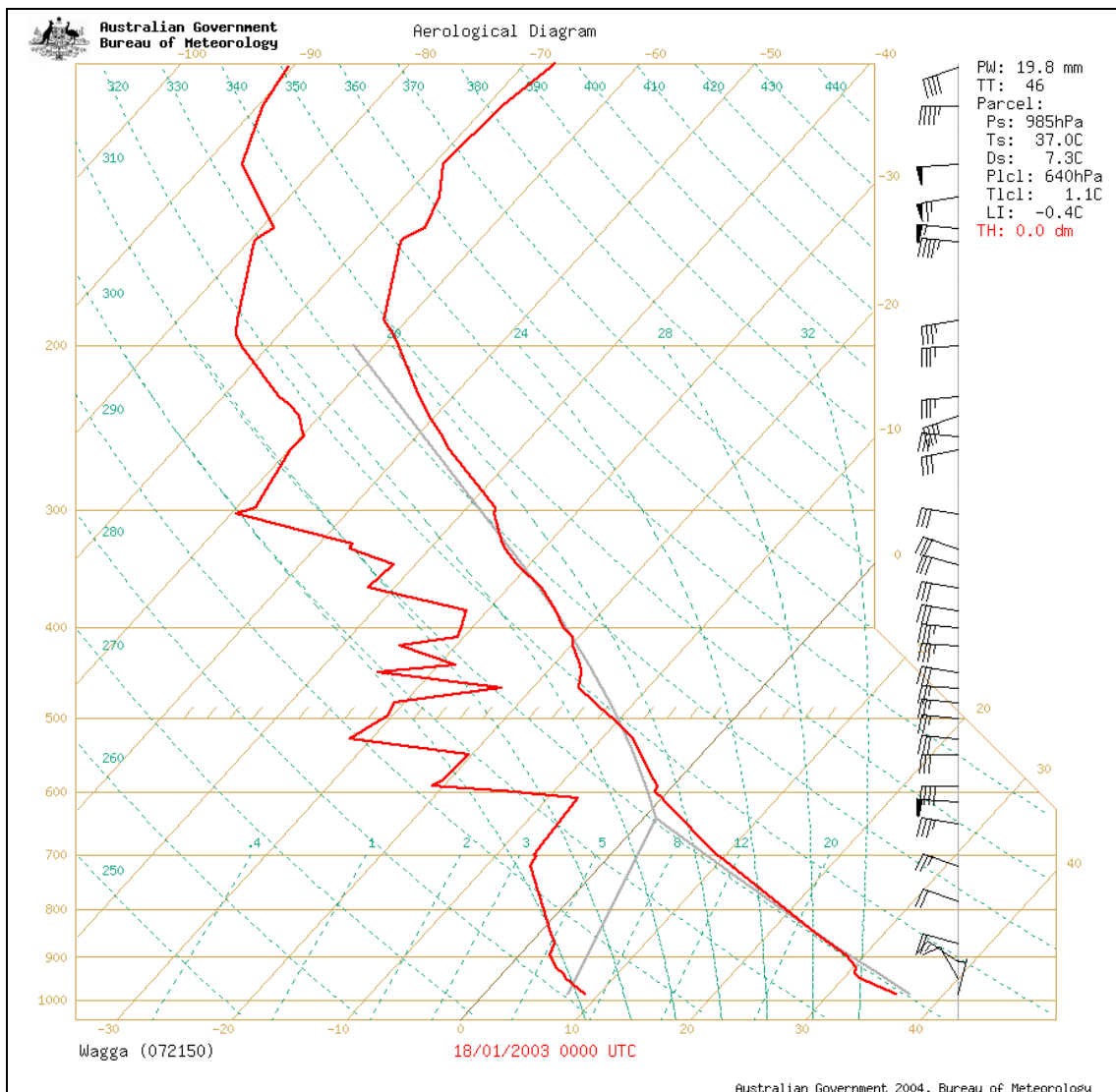


Figure 8. Upper-air sounding at Wagga for the flight at 0000 UTC 18 January 2003.

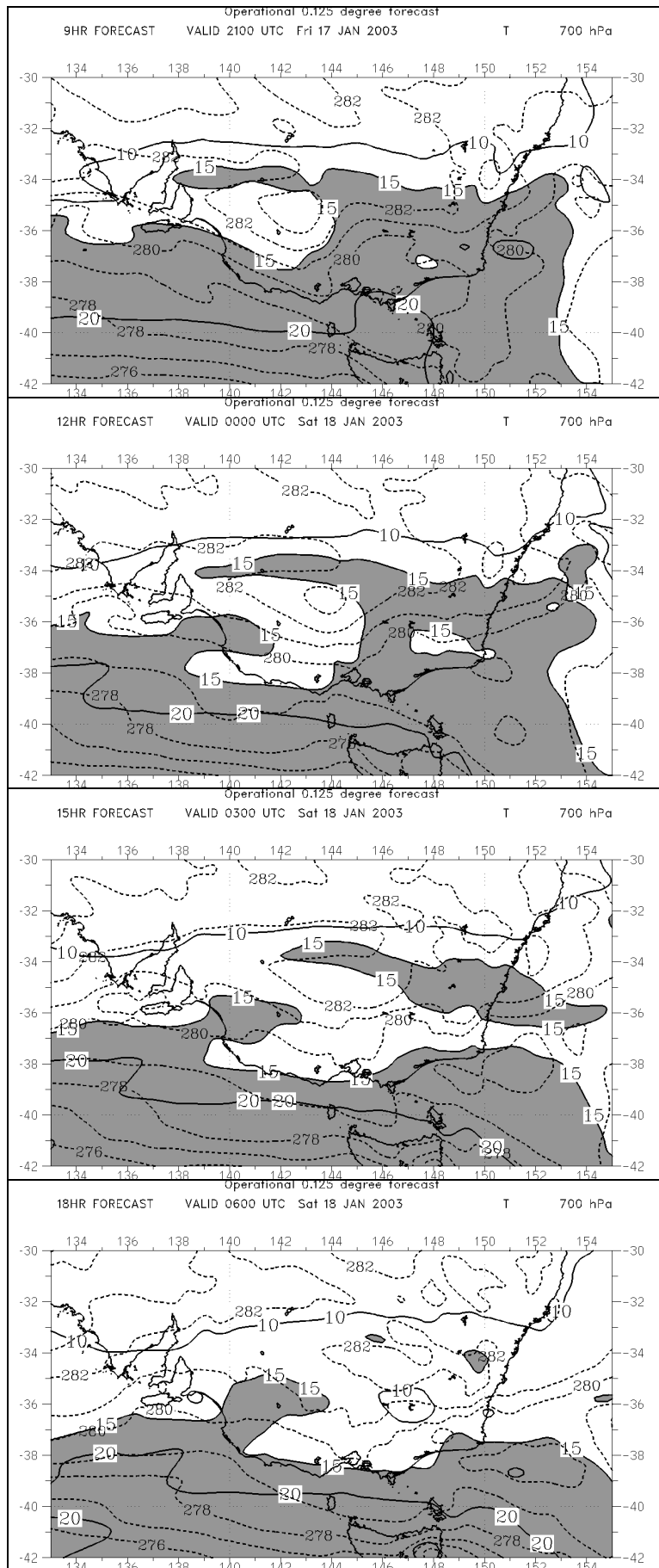


Figure 9. 700 hPa temperature and wind speed at 3-hourly intervals from the 0.125° meso-LAPS model, valid at 2100 UTC 17 January, and 0000, 0300, and 0600 UTC 18 January 2003. Temperature contours are dashed, at 1K intervals, while isotachs (heavy contours) are at 10, 15, and 20 m s^{-1} , with areas greater than 15 m s^{-1} shaded.

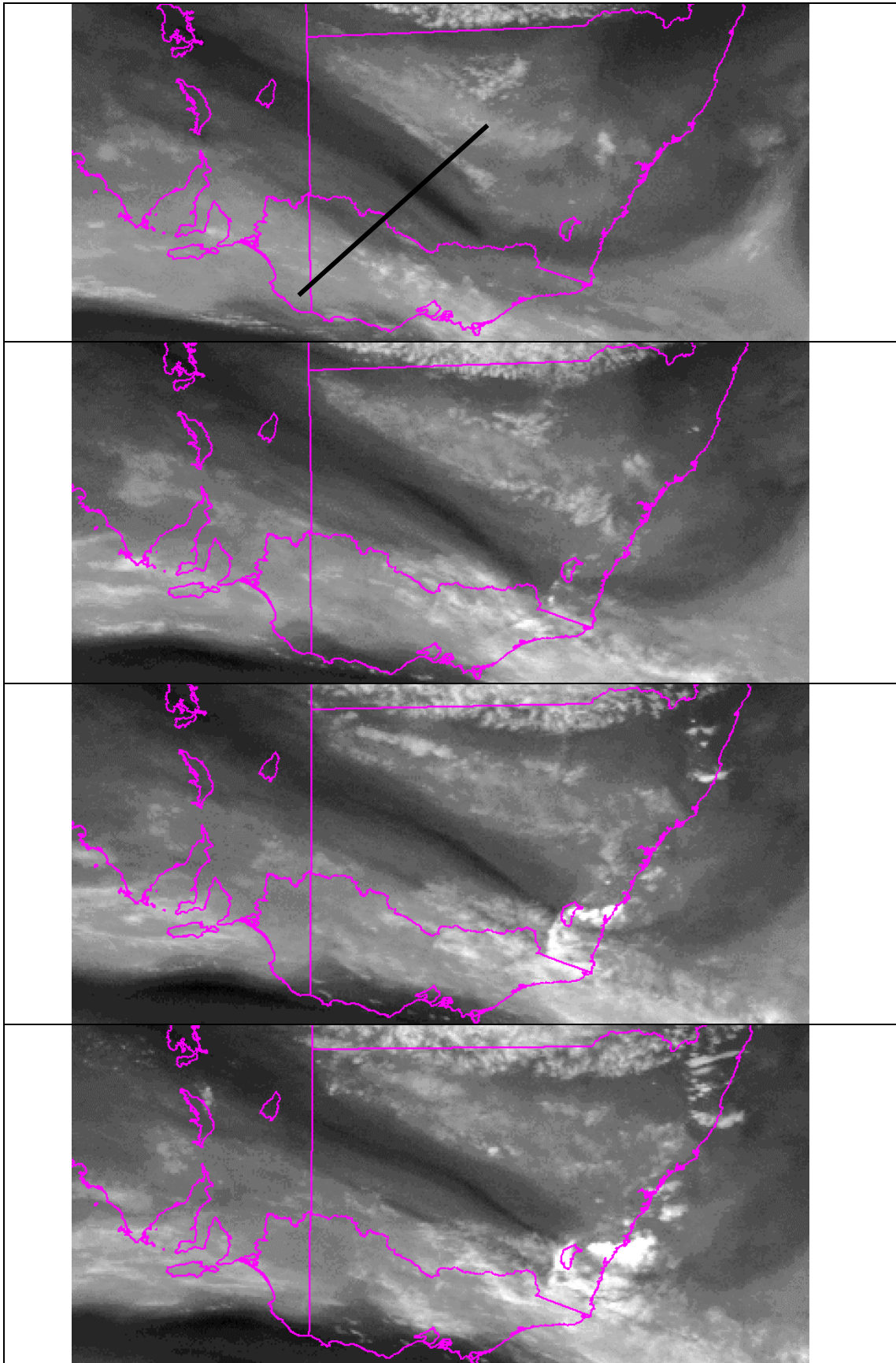


Figure 10. Enhanced Water-Vapour channel (6-7 μm) imagery from the GMS-5 satellite at 2330 UTC 17 January, and 0230, 0430, and 0530 UTC 18 January. The line in the upper panel marks the location of the cross-section in Fig. 11.

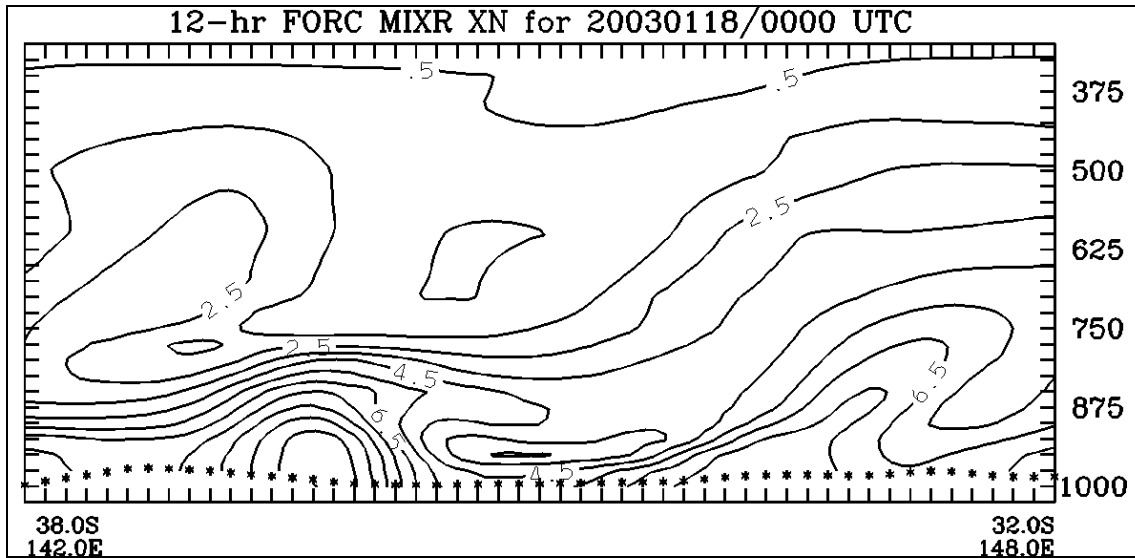


Figure 11. Mixing ratio cross section from the 0.125° meso-LAPS 12-hour forecast based at 1200 UTC 17 January 2003. Contour interval 1 gm Kg⁻¹.

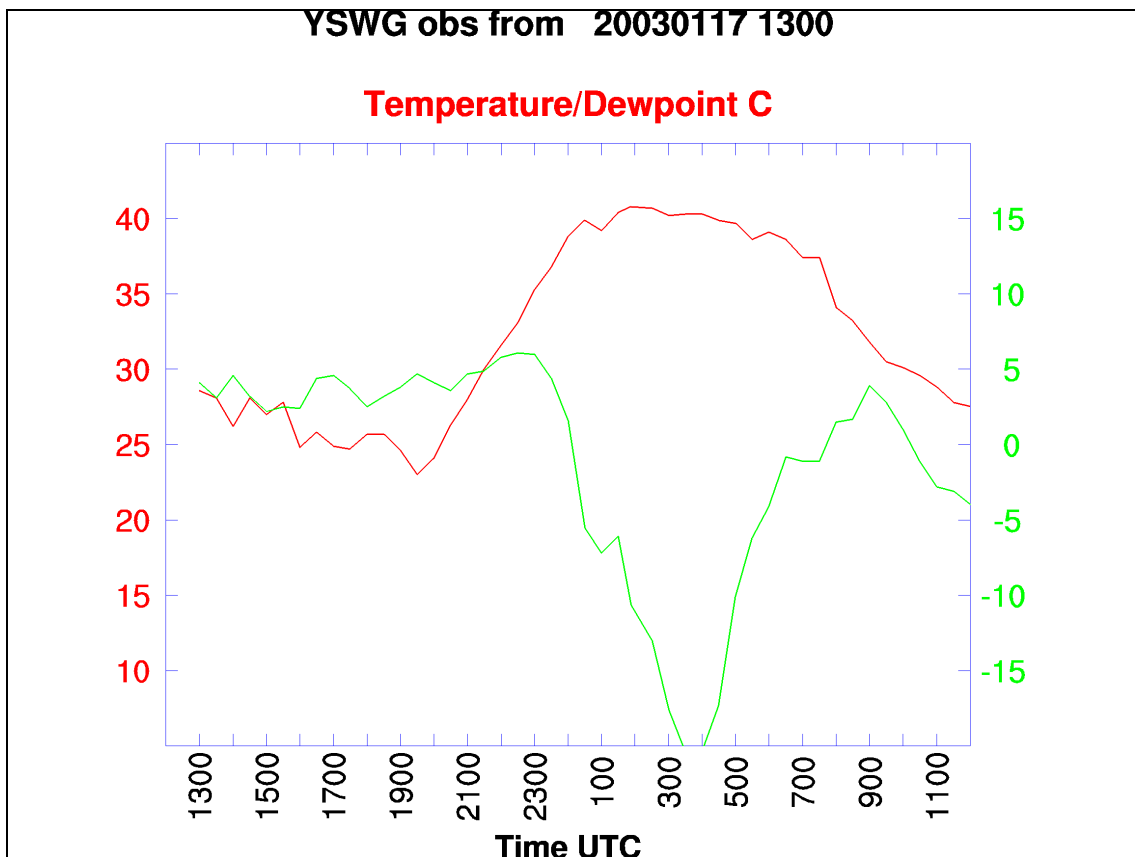


Figure 12. Time series of observations from Wagga (Fig. 1) from 1300 UTC 17 January 2003 to 1200 UTC 18 January 2003. Temperature (red) and dewpoint (green), both in C. Note the offset scales on the ordinates of the lower panel.

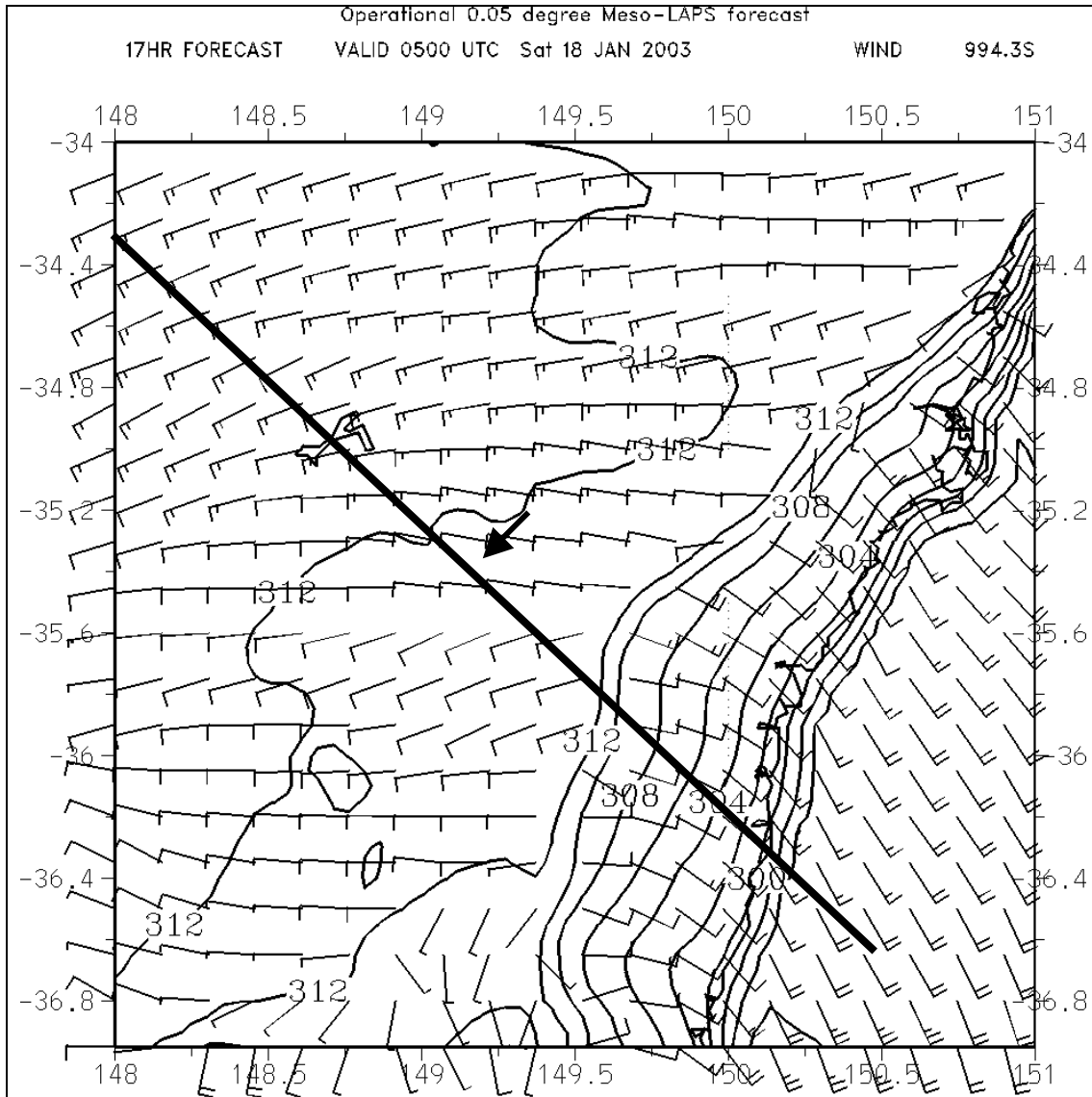


Figure 13. 0.05° meso-LAPS forecast of screen-level potential temperature and wind speed valid 0500 UTC 18 January 2003. The line marks the position of the vertical cross-sections shown in Fig 11, and the arrow indicates the location of Canberra.

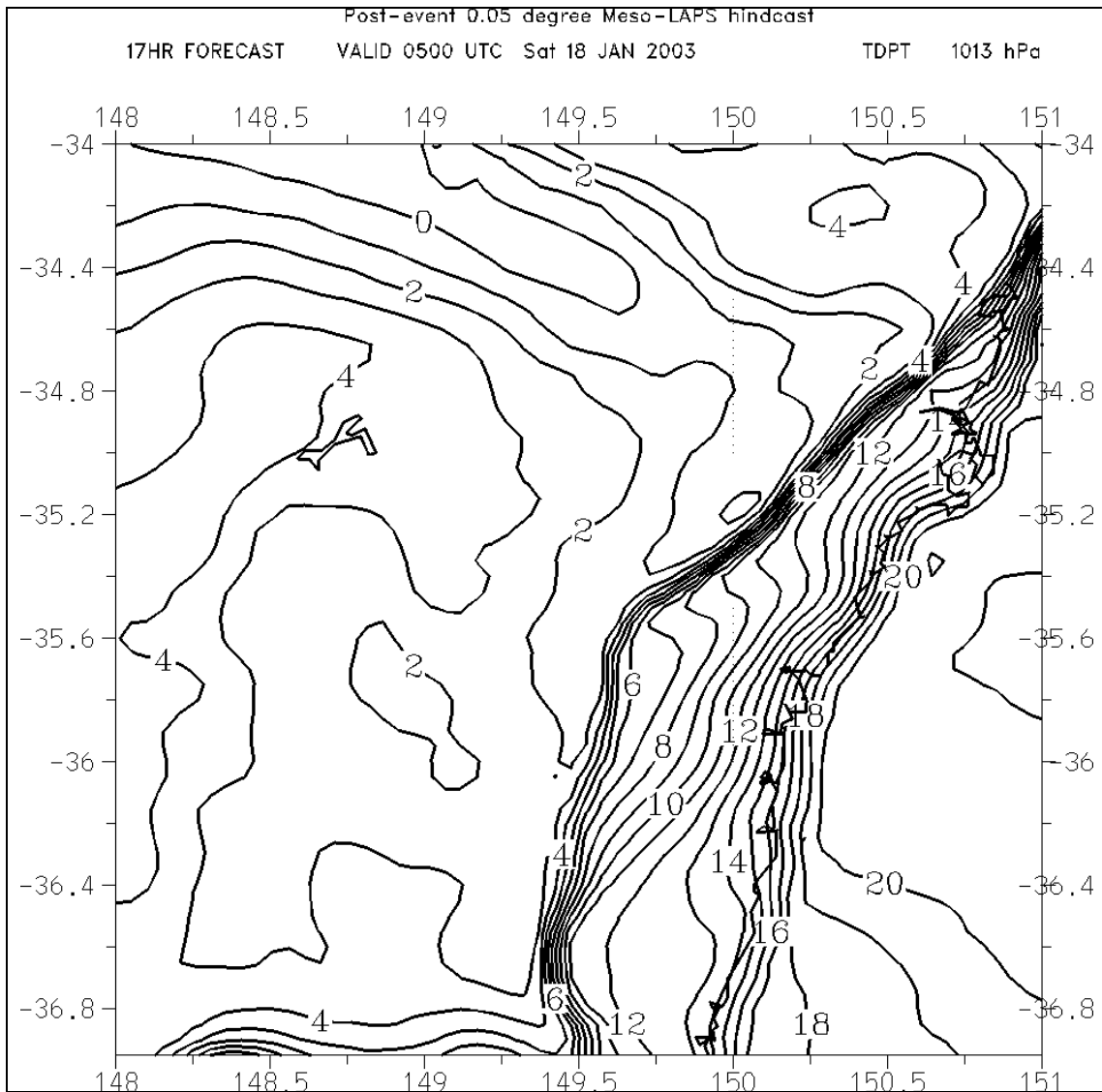


Figure 14. 0.05° meso-LAPS forecast of screen-level dewpoint (C) valid 0500 UTC 18 January 2003.

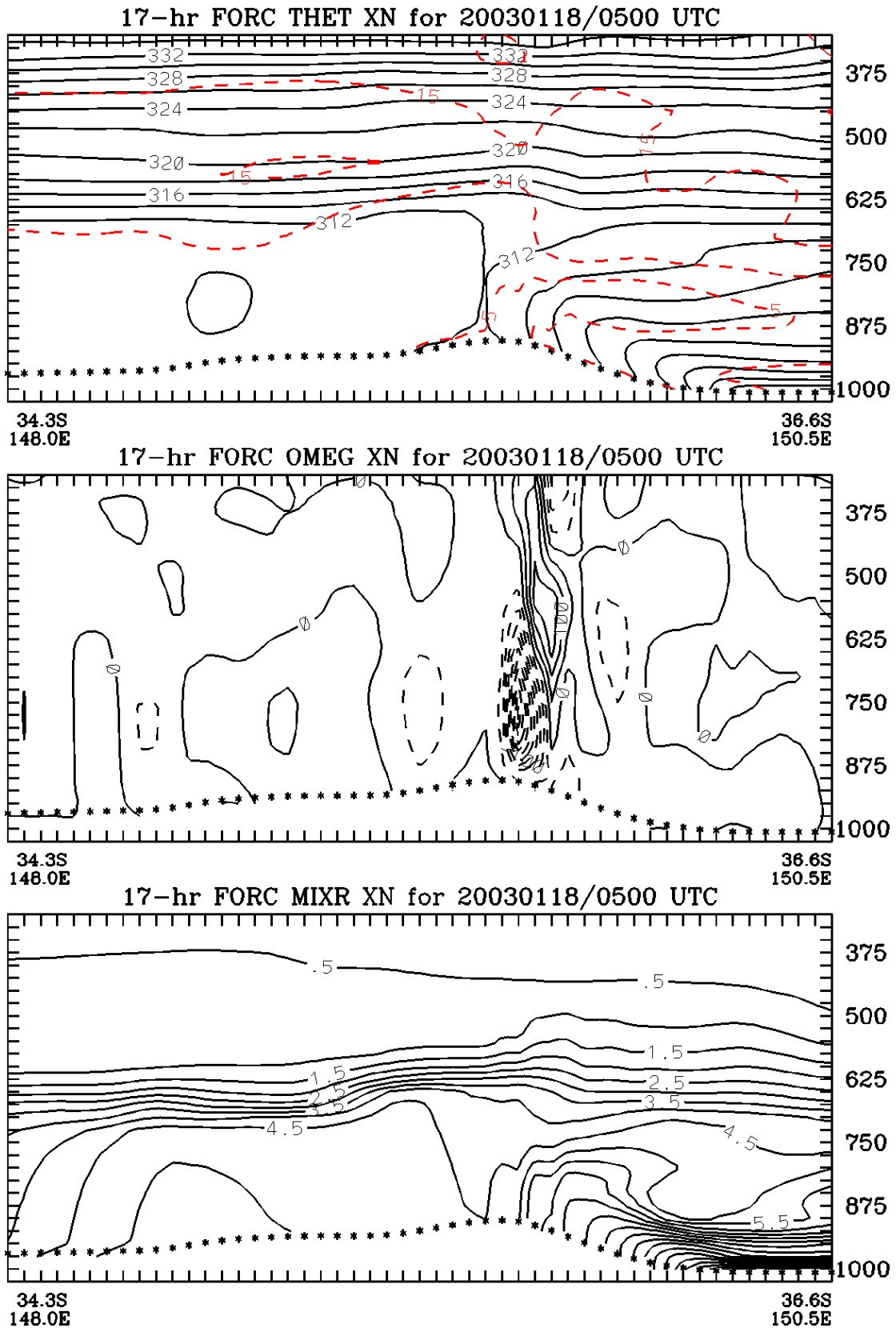


Figure 15. Cross-sections along the line in Fig 10. Upper panel shows potential temperature (solid, contour interval 2K) and wind speed (dashed, contour interval 5 ms^{-1}), middle panel vertical motion (hPa h r^{-1} , negative contours dashed), and lower panel mixing ratio (gm Kg^{-1}).

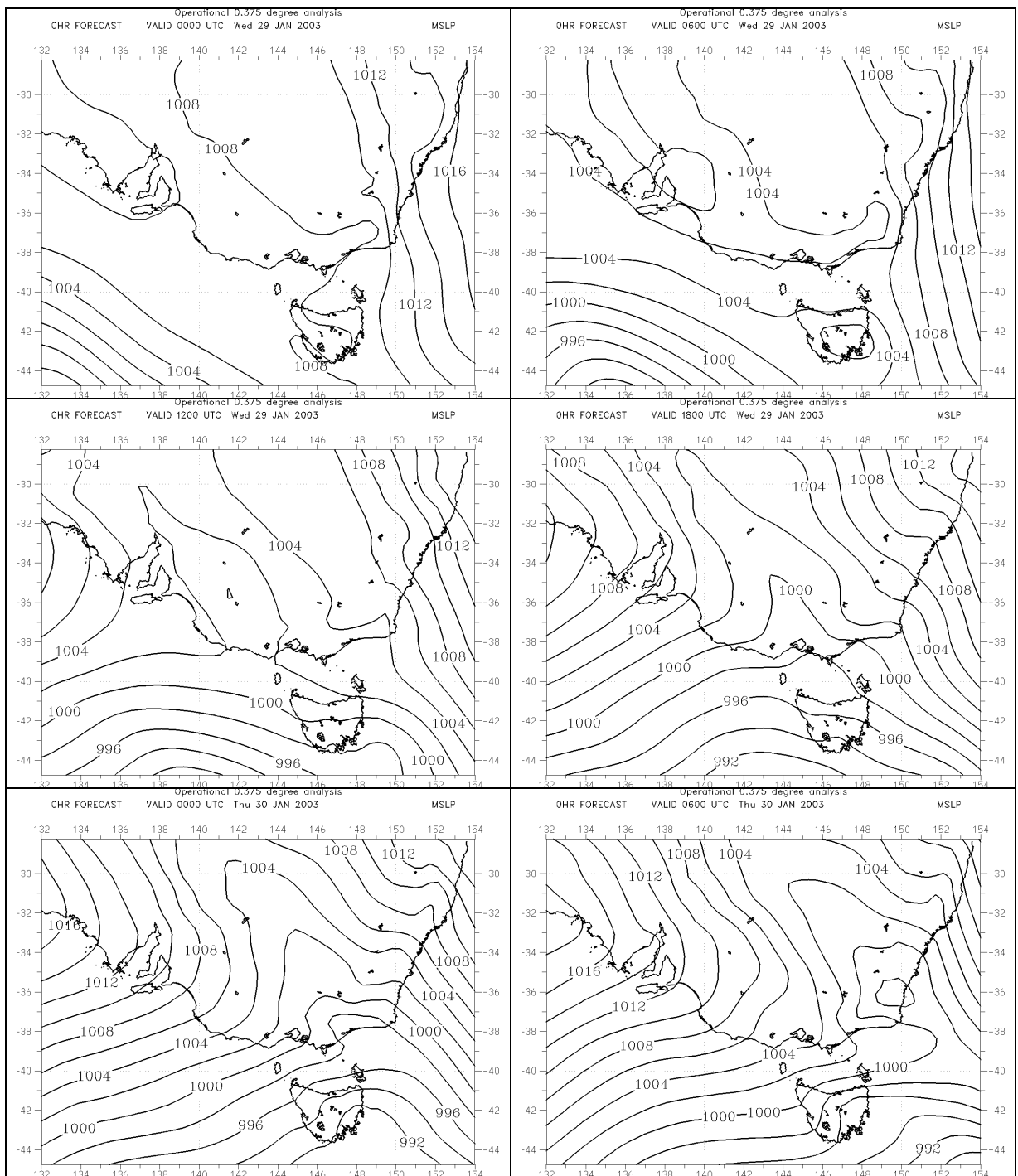


Figure 16. LAPS mean-sea-level pressure analyses from 0000 UTC 29 January to 0600 UTC 30 January 2003. Contour interval 2 hPa.

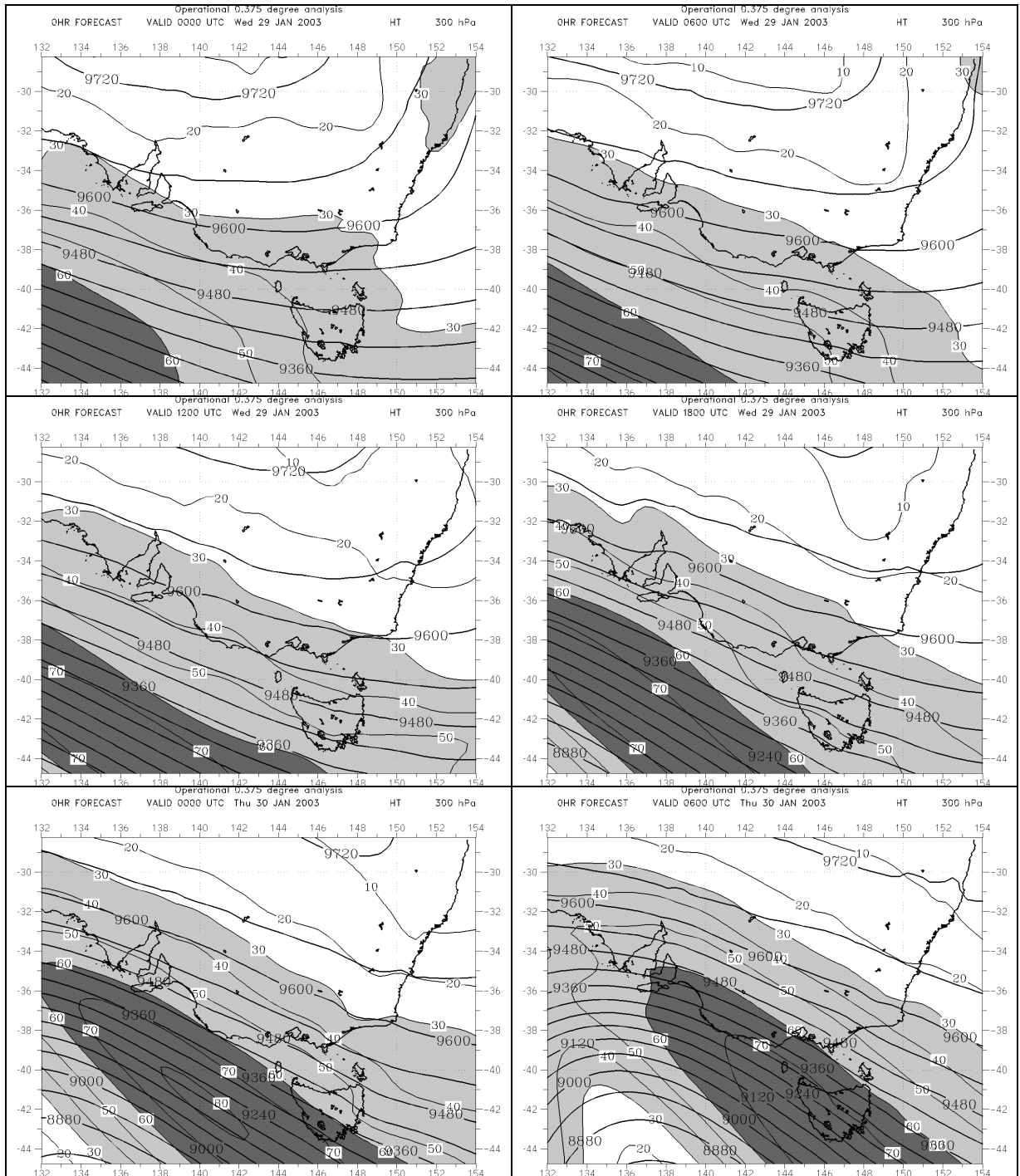


Figure 17. LAPS 300 hPa height/isotach analyses from 0000 UTC 29 January to 0600 UTC 30 January 2003. Geopotential height (heavy contours) at 60 gpm intervals, and isotachs (light contours) are shaded above 30 m s^{-1} (light) and 60 m s^{-1} (dark).

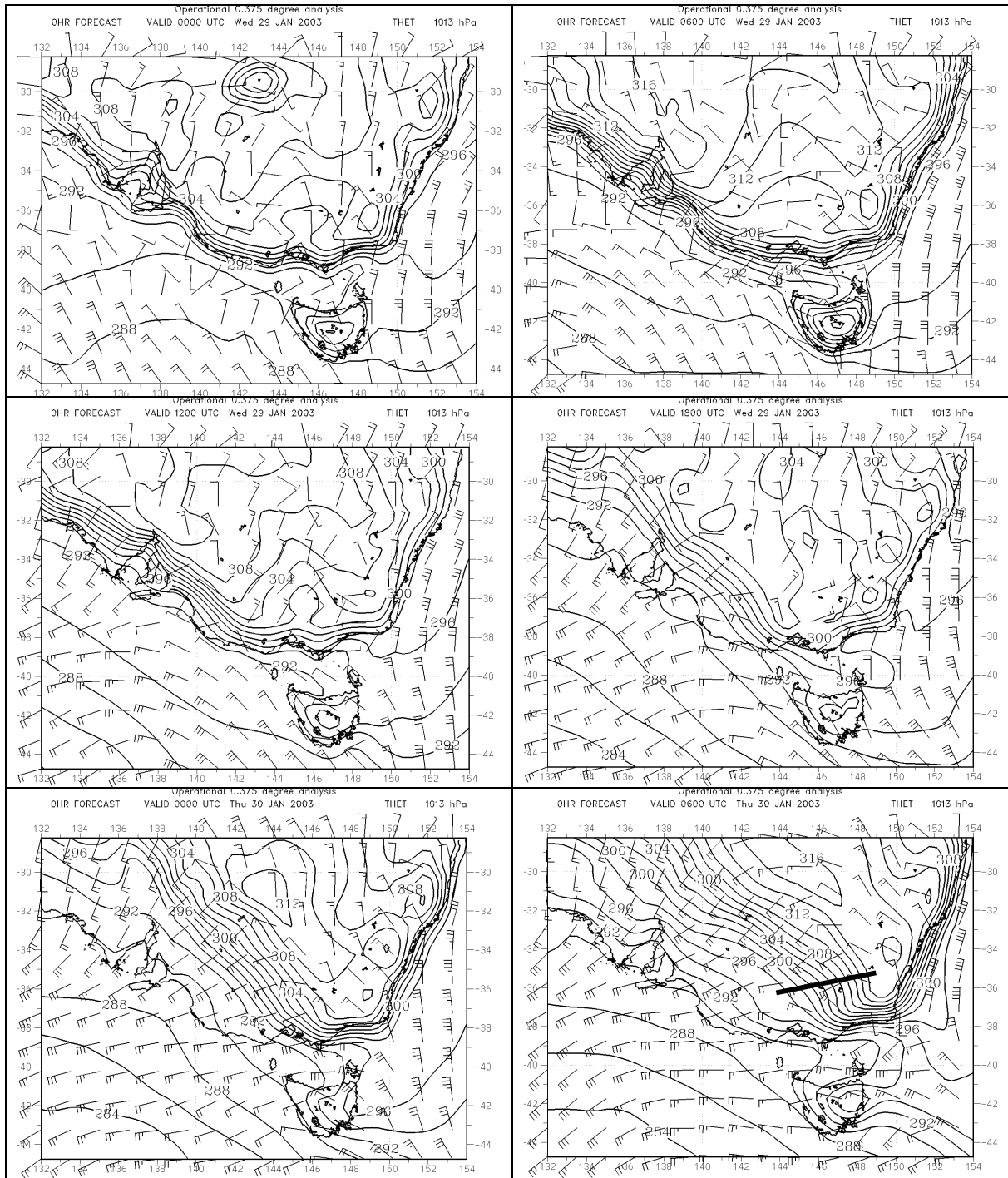


Figure 18. LAPS screen-level potential temperature and low-level wind speed analyses at 6-hour intervals from 0000 UTC 29 January to 0600 UTC 30 January 2003. Contour interval for potential temperature is 2K, while the wind barbs have their usual meteorological meaning. The line in the lower panel shows the locations of diagnostics and cross-sections in Figs. 25 and 26.

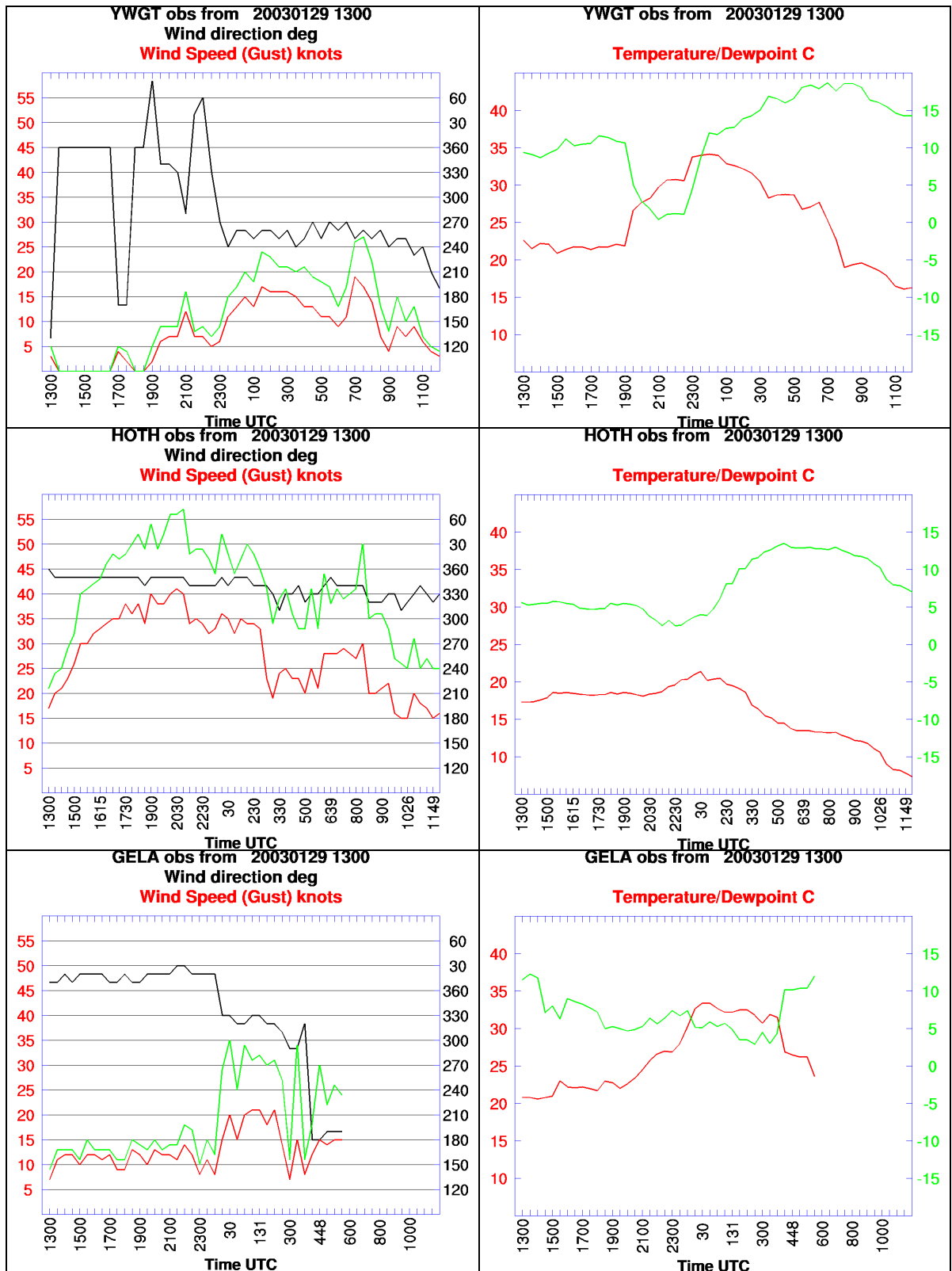


Figure 19. Time series of observations from Wangaratta (YWGT, see Fig. 1), Mt. Hotham (HOTH) and Gelantipy (GELA) from 1300 UTC 29 January 2003 to 1200 UTC 30 January 2003. Left panels – wind direction (degrees) in black, with wind speed and gust (knots) in red and green respectively. Right panels – temperature (red) and dewpoint (green), both in C. Note the offset scales on the ordinates of the right-hand panels.

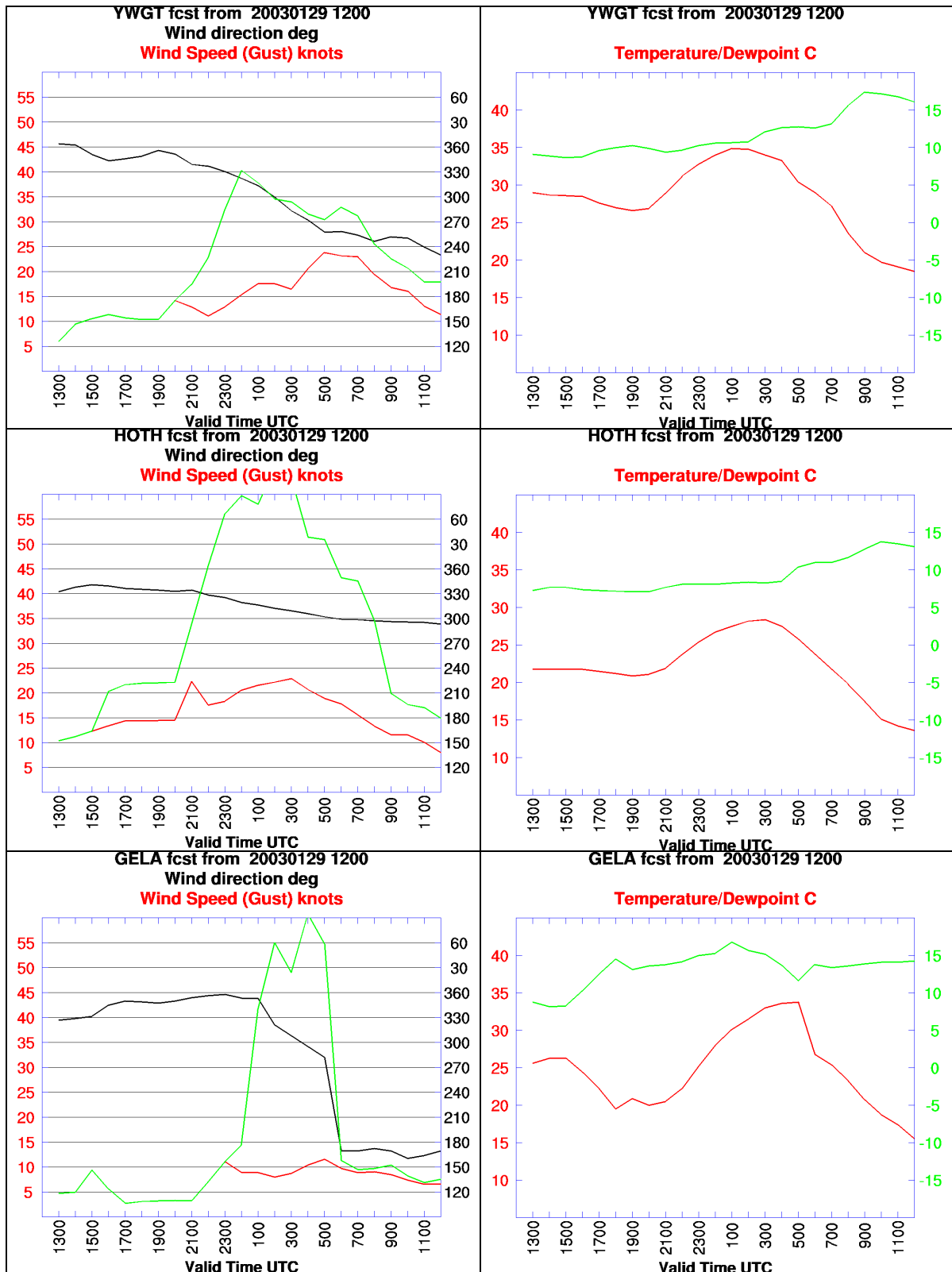


Figure 20. Time series of Melbourne-region 0.05° Meso-LAPS forecasts for Wangaratta (YWGT, see Fig. 1), Mt. Hotham (HOTH) and Gelantipy (GELA) from 1300 UTC 29 January 2003 to 1200 UTC 30 January 2003. Left panels – wind direction (degrees) in black, with wind speed and gust (knots) in red and green respectively. Right panels – temperature (red) and dewpoint (green), both in C. Note the offset scales on the ordinates of the right-hand panels.

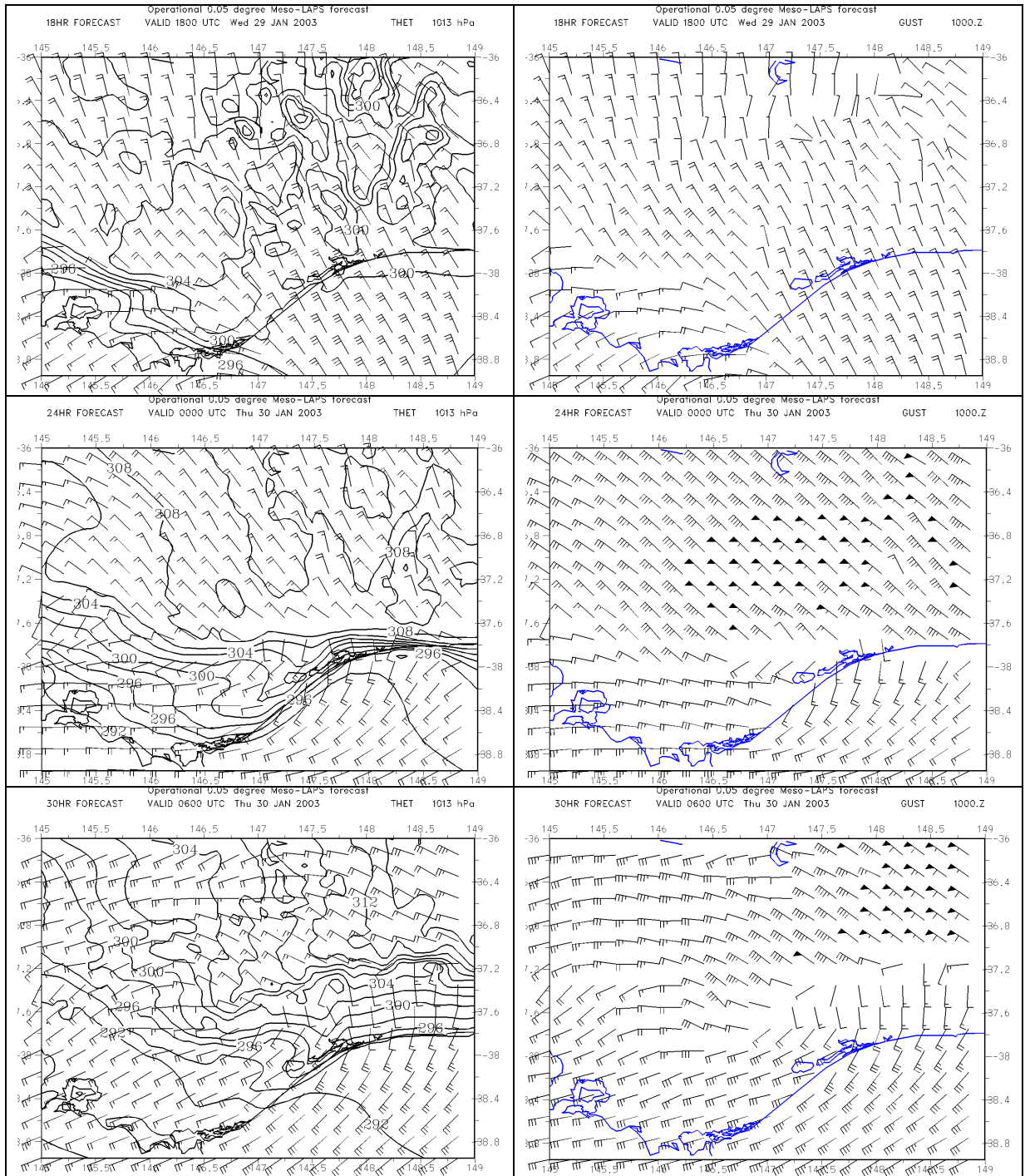


Figure 21. Screen-level potential temperature (contour interval 2K) overlaid with near-surface wind barbs (left column), and forecast surface wind gust (right column) for 18, 24 and 30-hour forecasts from the 0.05° meso-LAPS model run valid at 1800 UTC 29 January (top row), 0000 UTC (middle row) and 0600 UTC (bottom row) 30 January 2003.

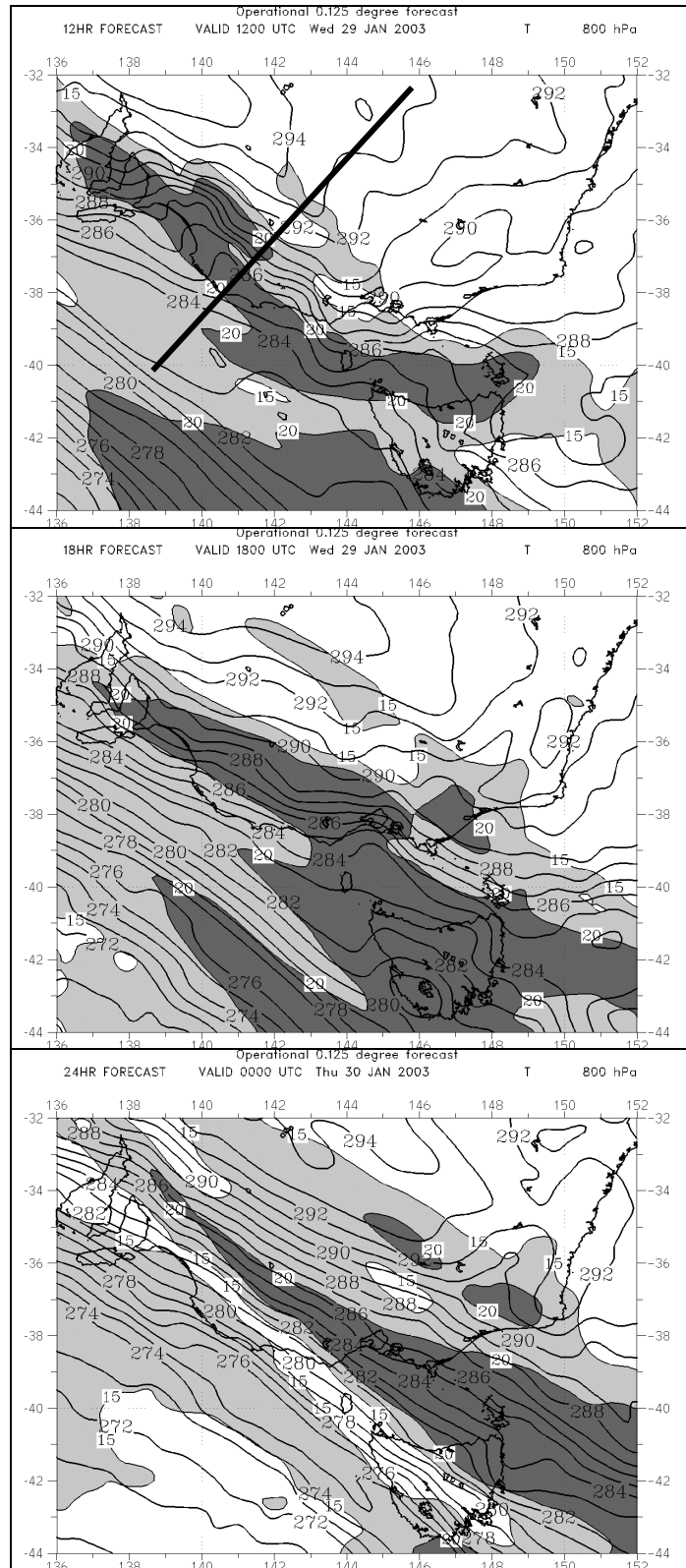


Figure 22. Forecast 800 hPa temperature and wind speed at 6-hourly intervals from the 0.125° meso-LAPS model, valid at 1800 UTC 29 January, and 0000 and 0600 UTC 30 January 2003. Temperature contours are at 1K intervals, while isotachs are shaded above 15 m s⁻¹ (light) and 20 m s⁻¹ (darker). The dark line in the upper panel shows the position of the cross-sections in Fig. 23.

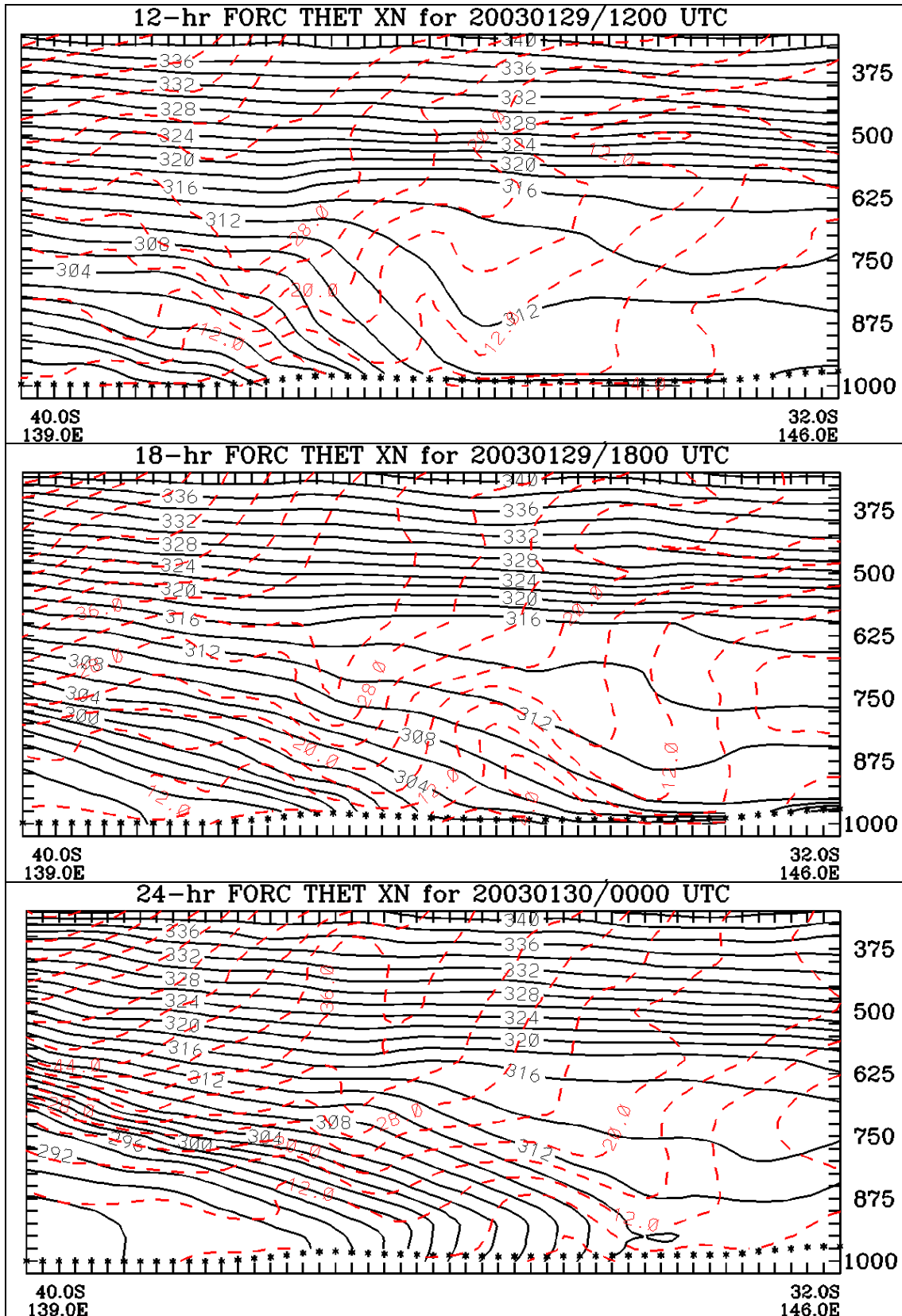


Figure 23. Cross-sections along the line shown in Fig. 22, valid at 1200 and 1800 UTC 29 January, and 0000 UTC 30 January 2003. Potential temperature (black) is contoured at 2K intervals, with wind speed (dashed red) at 5 m s⁻¹ intervals.

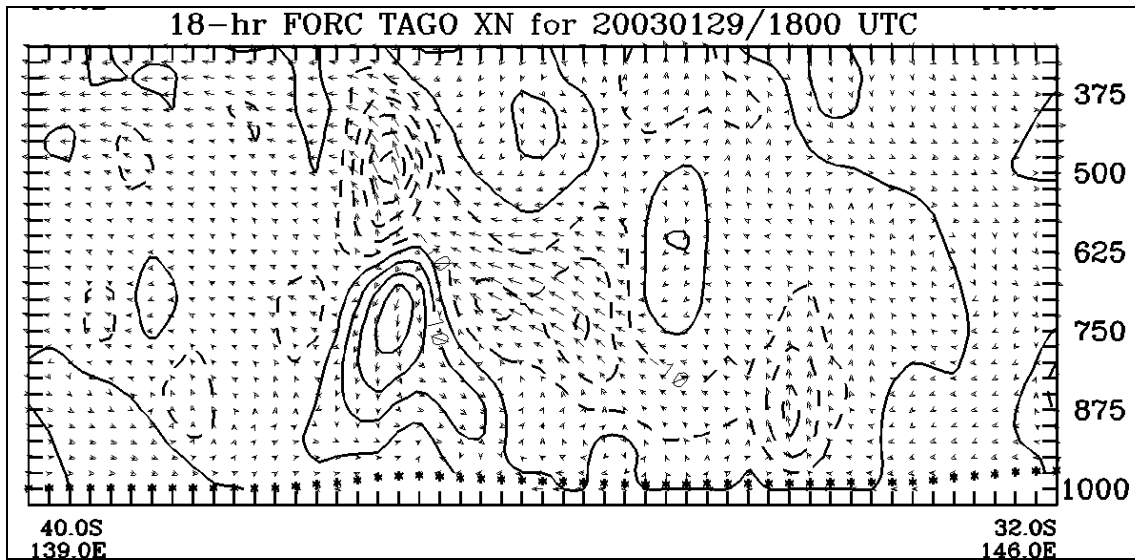


Figure 24. Cross-section, along the line shown in Fig. 22, valid at 1800 UTC 29 January, of the component of the ageostrophic wind vector in the plane of the section, with vertical motion (hPa/hr, negative values dashed) contoured.

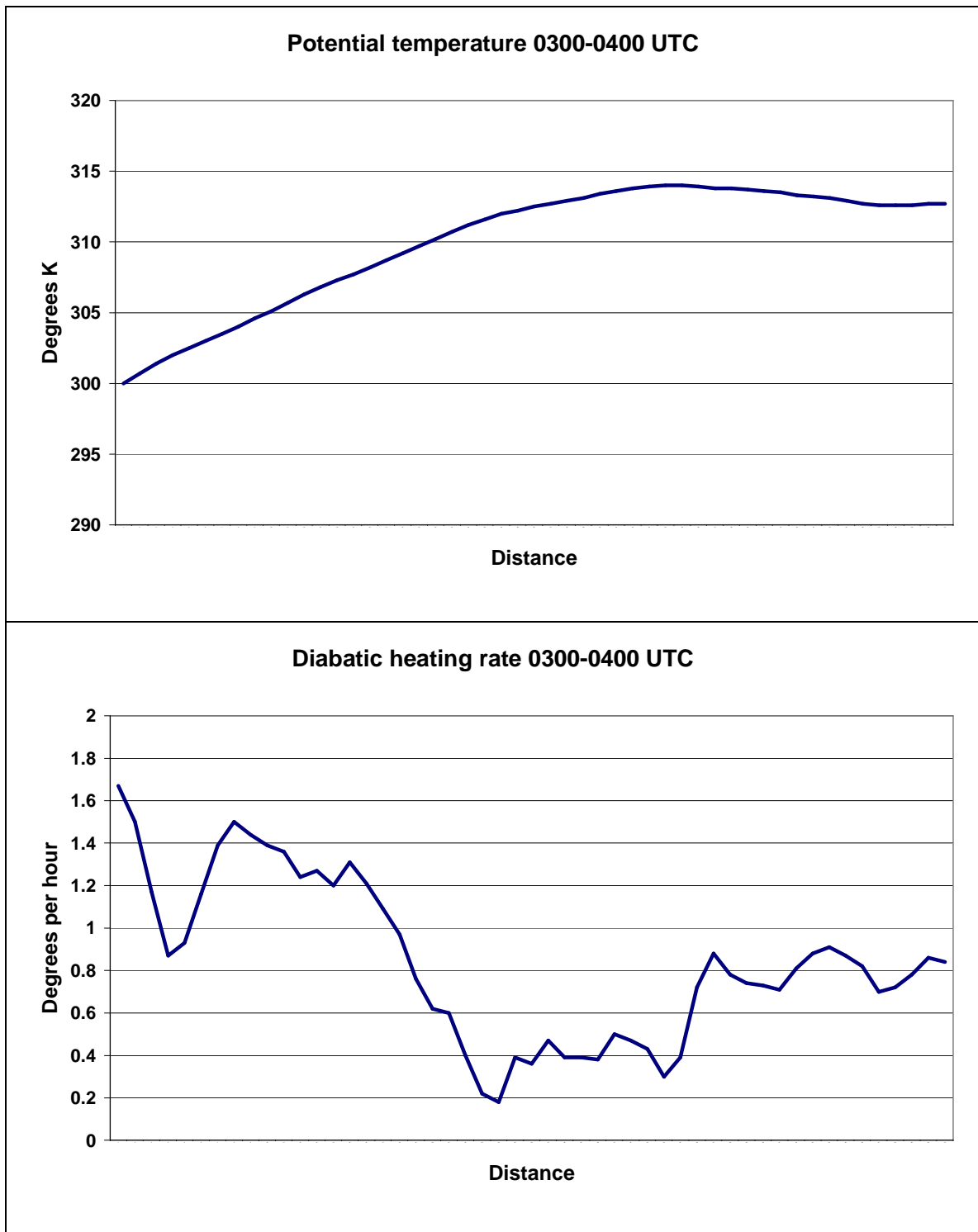


Figure 25. Upper panel – profile of forecast 950 hPa screen-level potential temperature at 0400 UTC 30 January 2003 along the line of the cross-sections shown in Fig. 18. Lower panel is the profile of the diabatic heating rate (K hr^{-1}) diagnosed from the forecast valid at 0300 and 0400 UTC along the same section.

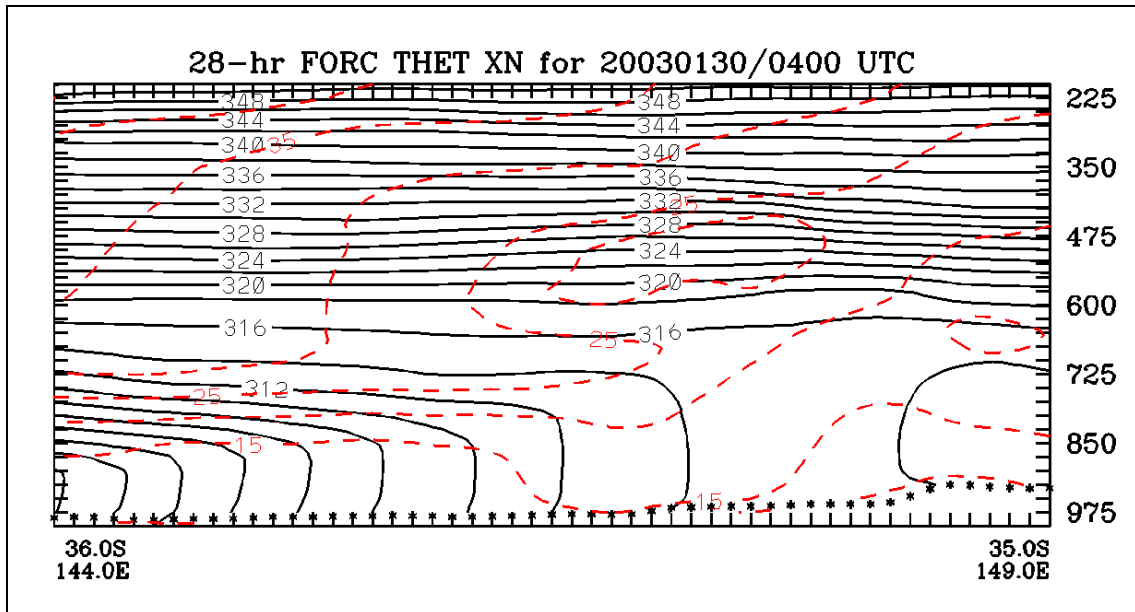


Figure 26. Cross-section of forecast potential temperature (solid contours, K) and wind speed (dashed contours, ms^{-1}) along the line of the section shown in Fig.18.